NASA/TM-2003-21621/Rev-Vol I

James L. Mueller, Giulietta S. Fargion and Charles R. McClain, Editors
J. L. Mueller, R.W. Austin, A. Morel, G.S. Fargion, and C.R. McClain, Authors.

Ocean Optics Protocols For Satellite Ocean Color Sensor Validation, Revision 4, Volume I:

Introduction, Background and Conventions

National Aeronautical and
Space administration

Goddard Space Flight Space Center
Greenbelt, Maryland 20771

January 2003

NASA/TM-2003-

Ocean Optics Protocols For Satellite Ocean Color Sensor Validation, Revision 4, Volume I:

Introduction, Background and Conventions

J. L. Mueller, and R.W. Austin
CHORS, San Diego State University, San Diego, California
Andre Morel
Laboratoire d'Oceanographie, Universite Pierre et Marie Curie, France
G.S. Fargion
Science Applications International Corporation, Beltsville, Maryland
C. R. McClain
Goddard Space Flight Center, Greenbelt, Maryland

National Aeronautical and
Space administration

Goddard Space Flight Space Center
Greenbelt, Maryland 20771

January 2003

Preface

This document stipulates protocols for measuring bio-optical and radiometric data for the Sensor Intercomparison and Merger for Biological and Interdisciplinary Oceanic Studies (SIMBIOS) Project activities and algorithm development. The document is organized into 7 separate volumes as:

Ocean Optics Protocols for Satellite Ocean Color Sensor Validation, Revision 4

Volume I: Introduction, Background and Conventions
Volume II: Instrument Specifications, Characterization and Calibration
Volume III: Radiometric Measurements and Data Analysis Methods
Volume IV: Inherent Optical Properties: Instruments, Characterization, Field Measurements and Data Analysis Protocols
Volume V: Biogeochemical and Bio-Optical Measurements and Data Analysis Methods
Volume VI: Special Topics in Ocean Optics Protocols
Volume VII: Appendices

The earlier version of *Ocean Optics Protocols for Satellite Ocean Color Sensor Validation*, *Revision 3* (Mueller and Fargion 2002, Volumes 1 and 2) is entirely superseded by the seven Volumes of Revision 4 listed above.

The new multi-volume format for publishing the ocean optics protocols is intended to allow timely future revisions to be made reflecting important evolution of instruments and methods in some areas, without reissuing the entire document. Over the years, as existing protocols were revised, or expanded for clarification, and new protocol topics were added, the ocean optics protocol document has grown from 45pp (Mueller and Austin 1992) to 308pp in Revision 3 (Mueller and Fargion 2002). This rate of growth continues in Revision 4. The writing and editorial tasks needed to publish each revised version of the protocol manual as a single document has become progressively more difficult as its size increases. Chapters that change but little, must nevertheless be rewritten for each revision to reflect relatively minor changes in, *e.g.*, cross-referencing and to maintain self-contained consistency in the protocol manual. More critically, as it grows bigger, the book becomes more difficult to use by its intended audience. A massive new protocol manual is difficult for a reader to peruse thoroughly enough to stay current with and apply important new material and revisions it may contain. Many people simply find it too time consuming to keep up with changing protocols presented in this format - which may explain why some relatively recent technical reports and journal articles cite Mueller and Austin (1995), rather than the then current, more correct protocol document. It is hoped that the new format will improve community access to current protocols by stabilizing those volumes and chapters that do not change significantly over periods of several years, and introducing most new major revisions as new chapters to be added to an existing volume without revision of its previous contents.

The relationships between the Revision 4 chapters of each protocol volume and those of Revision 3 (Mueller and Fargion 2002), and the topics new chapters, are briefly summarized below:

Volume I: This volume covers perspectives on ocean color research and validation (Chapter 1), fundamental definitions, terminology, relationships and conventions used throughout the protocol document (Chapter 2), requirements for specific *in situ* observations (Chapter 3), and general protocols for field measurements, metadata, logbooks, sampling strategies, and data archival (Chapter 4). Chapters 1, 2 and 3 of Volume I correspond directly to Chapters 1, 2 and 3 of Revision 3 with no substantive changes. Two new variables, Particulate Organic Carbon (POC) and Particle Size Distribution (PSD) have been added to Tables 3.1 and 3.2 and the related discussion in Section 3.4; protocols covering these measurements will be added in a subsequent revision to Volume V (see below). Chapter 4 of Volume I combines material from Chapter 9 of Revision 3 with a brief summary of SeaBASS policy and archival requirements (detailed SeaBASS information in Chapter 18 and Appendix B of Revision 3 has been separated from the optics protocols).

Volume II: The chapters of this volume review instrument performance characteristics required for *in situ* observations to support validation (Chapter 1), detailed instrument specifications and underlying rationale (Chapter 2) and protocols for instrument calibration and characterization standards and methods (Chapters 3 through 5). Chapters 1 through 5 of Volume II correspond directly to Revision 3 chapters 4 through 8, respectively, with only minor modifications.

Volume III: The chapters of this volume briefly review methods used in the field to make the *in situ* radiometric measurements for ocean color validation, together with methods of analyzing the data (Chapter 1), detailed measurement and data analysis protocols for in-water radiometric profiles (Chapter 2), above water measurements of remote sensing reflectance (Chapter III-3), determinations of exact normalized water-leaving radiance (Chapter 4), and atmospheric radiometric measurements to determine aerosol optical thickness and sky radiance distributions (Chapter 5). Chapter 1 is adapted from relevant portions of Chapter 9 in Revision 3. Chapter 2 of Volume III corresponds to Chapter 10 of Revision 3, and Chapters 3 through 5 to Revision 3 Chapters 12 through 14, respectively. Aside from reorganization, there are no changes in the protocols presented in this volume.

Volume IV: This volume includes a chapter reviewing the scope of inherent optical properties (IOP) measurements (Chapter 1), followed by 4 chapters giving detailed calibration, measurement and analysis protocols for the beam attenuation coefficient (Chapter 2), the volume absorption coefficient measured *in situ* (Chapter 3), laboratory measurements of the volume absorption coefficients from discrete filtered seawater samples (Chapter 4), and *in situ* measurements of the volume scattering function, including determinations of the backscattering coefficient (Chapter 5). Chapter 4 of Volume IV is a slightly revised version of Chapter 15 in Revision 3, while the remaining chapters of this volume are entirely new contributions to the ocean optics protocols. These new chapters may be significantly revised in the future, given the rapidly developing state-of-the-art in IOP measurement instruments and methods.

Volume V: The overview chapter (Chapter 1) briefly reviews biogeochemical and bio-optical measurements, and points to literature covering methods for measuring these variables; some of the material in this overview is drawn from Chapter 9 of Revision 3. Detailed protocols for HPLC measurement of phytoplankton pigment concentrations are given in Chapter 2, which differs from Chapter 16 of Revision 3 only by its specification of a new solvent program. Chapter 3 gives protocols for Fluorometric measurement of chlorophyll *a* concentration, and is not significantly changed from Chapter 17of Revision 3. New chapters covering protocols for measuring, Phycoerythrin concentrations, Particle Size Distribution (PSD) and Particulate Organic Carbon (POC) concentrations are likely future additions to this volume.

Volume VI: This volume gathers chapters covering more specialized topics in the ocean optics protocols. Chapter 1 introduces these special topics in the context of the overall protocols. Chapter 2 is a reformatted, but otherwise unchanged, version of Chapter 11 in Revision 3 describing specialized protocols used for radiometric measurements associated with the Marine Optical Buoy (MOBY) ocean color vicarious calibration observatory. The remaining chapters are new in Revision 4 and cover protocols for radiometric and bio-optical measurements from moored and drifting buoys (Chapter 3), ocean color measurements from aircraft (Chapter 4), and methods and results using LASER sources for stray-light characterization and correction of the MOBY spectrographs (Chapter 5). In the next few years, it is likely that most new additions to the protocols will appear as chapters added to this volume.

Volume VII: This volume collects appendices of useful information. Appendix A is an updated version of Appendix A in Revision 3 summarizing characteristics of past, present and future satellite ocean color missions. Appendix B is the List of Acronyms used in the report and is an updated version of Appenix C in Revision 3. Similarly, Appendix C, the list of Frequently Used Symbols, is an updated version of Appendix D from Rev. 3. The SeaBASS file format information given in Appendix B of Revision 3 has been removed from the protocols and is promulgated separately by the SIMBIOS Project.

In the Revision 4 multi-volume format of the ocean optics protocols, Volumes I, II and III are unlikely to require significant changes for several years. The chapters of Volume IV may require near term revisions to reflect the rapidly evolving state-of-the-art in measurements of inherent optical properties, particularly concerning instruments and methods for measuring the Volume Scattering Function of seawater. It is anticipated that new chapters will be also be added to Volumes V and VI in Revision 5 (2003).

This technical report is not meant as a substitute for scientific literature. Instead, it will provide a ready and responsive vehicle for the multitude of technical reports issued by an operational Project. The contributions are published as submitted, after only minor editing to correct obvious grammatical or clerical errors.

Table of Contents and Author List

Chapter 1

Ocean Color Radiometry and Bio-Optics

James L. Mueller[1], Roswell W. Austin[1], Giulietta S. Fargion[2] and Charles R. McClain[3]
[1]*Center for Hydro-Optics and Remote Sensing, San Diego State University, California*
[2]*Science Applications International Corporation, Beltsville, Maryland*
[3]*NASA, Goddard Space Flight Center, Greenbelt, Maryland*

1.1 INTRODUCTION

During the period from *circa* 1985 to 1991, the National Aeronautics and Space Administration (NASA) charged a series of successive science working groups with the task of recommending guidelines, goals and mission design criteria for future satellite ocean color remote sensors. The deliberations of these working groups were based on the ocean color science community's experiences with the Nimbus-7 Coastal Zone Color Scanner (CZCS). On the one hand, the highly successful CZCS mission firmly established ocean color remote sensing as a powerful tool for monitoring and studying the bio-optical properties of the global ocean. On the other hand, the radiometric responsivities of the CZCS channels declined progressively with time throughout its 8-year operating life, which just as firmly established the need to independently verify a satellite sensor's performance using *in situ* measurements of the ocean and atmosphere. From those two general perspectives, the principal recommendations of these NASA Ocean Color Science Working Groups (collectively) included:

1. ***Baseline satellite ocean color products*** should include
    a. Normalized water-leaving radiances $L_{WN}(\lambda)$ (Gordon and Clark, 1981),
    b. Aerosol radiances $L_a(\lambda)$,
    c. Chlorophyll *a* concentration $Chl\left[\text{mg m}^{-3}\right]$,
    d. The diffuse attenuation coefficient $K(490)$ at a wavelength of 490 nm, and
    e. Calibrated radiances $L_t(\lambda)$ observed at the satellite.
2. ***Principal goals for product uncertainties*** should be
    a. Less than ***5 % uncertainty*** in $\boldsymbol{L_{WN}(\lambda)}$ and
    b. Less than ***35 % uncertainty*** in ***Chl***.
3. An ***ongoing satellite ocean color sensor system validation program*** is necessary, using *in situ* measurements of ocean radiometric and bio-optical properties, and of atmospheric optical properties, to verify system performance - including algorithms - immediately after launch and throughout a satellite ocean color sensor's operating lifetime.

These and other recommendations of the earlier working groups were endorsed by the Sea-viewing Wide Field-of-view Sensor (SeaWiFS) Science Team and accepted by NASA. Of particular significance in the present context, the SeaWiFS Project Office moved immediately to implement a SeaWiFS Validation Plan designed to assure a best effort to achieve the above product uncertainty goals (McClain *et al.* 1992). A critical aspect of the validation plan was that *in situ* radiometric, optical and bio-optical measurements of uniformly high quality and accuracy be obtained for verifying SeaWiFS system performance and product uncertainties. Therefore, in 1991 the SeaWiFS Project Office sponsored a workshop to recommend appropriate measurements, instrument specifications, and protocols specifying methods of calibration, field measurements, and data analysis necessary to support SeaWiFS validation, leading to the first publication of *Ocean Optics Protocols for SeaWiFS Validation* (Mueller and Austin

1992). Continued discourse within the ocean color research community led to Revisions 1 (Mueller and Austin 1995), 2 (Fargion and Mueller 2000) and 3 (Mueller and Fargion 2002) of these protocols.

The Ocean Optics Protocols for Satellite Ocean Color Sensor Validation (Revision 4.0) are intended to provide standards, which if followed carefully and documented appropriately, will assure that any particular set of optical measurements will be acceptable for ocean color sensor validation and algorithm development. These protocols are guidelines and may be somewhat conservative. In the case of ship shadow avoidance, for example, there are some circumstances in which acceptable radiometric profiles may be acquired considerably closer to a ship than is specified here in Volume III, Chapter 2 (Section 2.2). When the protocols are not followed in such cases, however, it is incumbent upon the investigator to explicitly demonstrate that the actual error levels are within tolerance. Close adherence to these protocols is the most straightforward way for an investigator to establish a measurement that is uncontaminated by artifacts, such as ship shadow, and is accurate enough to meet the requirements of satellite ocean color product validation.

Finally, having a standard set of measurement protocols is indispensable in developing consistency across the variety of international satellite ocean color missions either recently launched or scheduled for launch in the next few years. While each mission has its own validation effort, the mission validation teams should not need to define separate validation measurement requirements. In the U.S., for instance, ocean color validation support is derived from four separate funding programs, i.e., the SeaWiFS Project, Moderate Resolution Imaging Spectroradiometer (MODIS) validation program, the Earth Observing System (EOS) calibration and validation program, and the Sensor Intercomparison for Marine Biology and Interdisciplinary Oceanic Studies (SIMBIOS) Project (McClain and Fargion, 1999a, 1999b). Continued development and refinement of these protocols help ensure coordination, collaboration, and communication between those involved.

1.2 OBJECTIVES

Immediate concerns focused the early versions of the Ocean Optics Protocols (Mueller and Austin 1992, 1995) on specific preparations for the SeaWiFS mission. In the interim, not only SeaWiFS, but the Japanese Ocean Color Temperature Sensor (OCTS), the Polarization Detection Environmental Radiometer (POLDER), and the MODIS global coverage ocean color systems have been successfully launched and brought into operation, and the near-term launch of several other such systems is anticipated (Appendix A). The SIMBIOS Program goal is to assist the international ocean color community in developing a multi-year time-series of calibrated radiances that transcends the spatial and temporal boundaries of individual missions (Barnes *et al.* 2001). Specific objectives are to: (1) quantify the relative accuracies of the products from each mission, (2) work with each project to improve the level of confidence and compatibility among the products, and (3) develop methodologies for generating merged level-3 products. SIMBIOS has identified the primary instruments to be used for developing global data sets. These instruments are SeaWiFS, OCTS, POLDER [Advanced Earth Observing Satellite (ADEOS)-I and II], MODIS (Terra and Aqua), Multi-angle Imaging SpectroRadiometer (MISR), Medium Resolution Imaging Spectrometer (MERIS), and Global Line Imager (GLI). The products from other missions [e.g., Ocean Color Imager (OCI), Ocean Scanning Multisprectral Imager (OSMI), and Modular Optoelectronic Scanner (MOS)] will be tracked and evaluated, but are not considered as key data sources for a combined global data set.

The scope of the protocols was, therefore, broadened to support development of bio-optical databases that meet the expanded requirements of the SIMBIOS goals and objectives (Fargion and Mueller 2000). The key objective addressed by the original working group was to recommend protocols and standards for supporting *in situ* optical measurements. The original objectives remain valid today, albeit with broader requirements for detailed measurements and sensor characteristics (e.g. wavelength characteristics). The generalized protocol objectives address the following subject areas:

1. The required and useful optical parameters to be used for validation of satellite ocean color sensor normalized water-leaving radiances and atmospheric correction algorithms, and for monitoring each satellite sensor's calibration and stability, will be defined.
2. The instrumentation requirements, and standards for measuring the parameters in item 1, including definitions of measured quantities, wavelengths, field-of-view (FOV) and band specifications, sensitivity, uncertainty and stability, will be delineated.

3. The optical instrument characterization, intercalibration standards, and related protocols will be defined. This objective includes the following subjects:

    a) laboratory calibration and characterization measurements, uncertainties, and procedures to be applied to instruments used in satellite ocean color sensor validation and algorithm development activities;

    b) pre- and post-deployment measurements and procedures to be followed with moored instrumentation; and

    c) methods for instrument calibration and characterization, and the requirements for record keeping and traceability, including intercalibrations of radiometric and optical standards between participating laboratories.

4. The at-sea optical sampling strategy and protocols will be standardized. This objective includes such considerations as:

    a) the rationale and justifications for moored, underway, drifting, shipboard, and airborne measurements;

    b) ship shadow avoidance, depth resolution in optical profiles, and total sampling depths; and

    c) time of day, sky conditions, season, and geographic considerations.

5. The analysis approaches to be used shall be refined. This objective includes recommended procedures and methodologies for generating derived variables from *in situ* observations, for example normalized water-leaving radiance $L_{\mathrm{WN}}(\lambda)$ (Gordon and Clark 1981) and exact normalized water-leaving radiance $L_{\mathrm{WN}}^{\mathrm{ex}}(\lambda)$ (Morel and Gentili 1996; Volume III, Chapter 4) from $L_{\mathrm{u}}(z,\lambda)$, and $K_{\mathrm{d}}(z,\lambda)$ from $E_{\mathrm{d}}(z,\lambda)$.

6. Protocols for ancillary measurements, data archiving, database population, and access to data will be standardized.

7. The required atmospheric measurements will be defined, and the degree to which standard methodologies are available will be evaluated.

Specific methods for development and validation of bio-optical algorithms for ocean color sensors are only briefly examined in this report. Nonetheless, the scope of the optics protocols includes data requirements and sampling strategies for bio-optical and radiometric measurements supporting these activities. This topic includes the following subjects:

1. Discrete chlorophyll *a* and pigment concentrations will be measured using for high performance liquid chromatography (HPLC) pigment sampling and analysis, protocols and standards for which closely follow those adopted by the Joint Global Ocean Flux Study (JGOFS) (UNESCO 1994). These protocols are presented here in Volume V, Chapter 2.

2. An assessment will be made of the roles of underway, moored, and discrete fluorescence measurements, how such measurements are calibrated, and their usefulness for satellite data product validation. Protocols are included for fluorometric measurement of chlorophyll *a* concentration (Volume V, Chapter 3), again closely following the counterpart JGOFS protocols (UNESCO 1994).

3. The need for biogeochemical measurements of colored dissolved organic material (CDOM), coccoliths, suspended sediment, detritus, etc., will be examined on the basis of baseline product requirements. Protocols are included here (Volume IV, Chapter 4) for *in situ* and laboratory measurements of spectral absorption by CDOM, and by suspended particles. The other aspects of this topic are addressed in more general terms.

1.3 SENSOR CALIBRATION

The individual satellite sensor project offices, as well as the SIMBIOS Project, must make every effort to track the sensor's performance throughout the duration of the mission. Since SeaWiFS, for example, is designed for a five-year mission, it was certain from the outset that the sensor calibration at each wavelength would change in some unpredictable manner as a function of time. Experience with the CZCS showed it is very difficult to determine a sensor's calibration once it has been launched (Viollier 1982, Gordon *et al.* 1983, Hovis *et al.* 1985, Mueller 1985, Gordon 1987, and Evans and Gordon 1994). Similar problems have been encountered with other earth observing systems, such as the National Oceanic and Atmospheric Administration (NOAA) Advanced Very High Resolution Radiometer (AVHRR) (Brown and Evans 1985 and Weinreb *et al.* 1990). Because of the large atmospheric contribution to the total observed radiances (Gordon 1981) and the great sensitivity of the bio-optical algorithms to the estimated water-leaving radiances (Clark 1981), small errors in the calibration can induce sizable errors in derived geophysical products, rendering them useless for many applications.

By processing large quantities of so-called "clear-water" imagery, *i.e.* in water with pigment concentrations less than 0.25 mg m^{-3} (Gordon and Clark 1981), Evans and Gordon (1994) were able to develop a vicarious calibration that was used in the global processing of the entire CZCS data set (Esaias *et al.* 1986, Feldman *et al.* 1989 and McClain *et al.* 1993). The approach, however, required assumptions that may limit the scientific utility of ocean color imagery. Specifically, the normalized clear water-leaving radiances, $L_{WN}(443)$, $L_{WN}(520)$, and $L_{WN}(550)$, were assumed to be 1.40, 0.48, and 0.30 mW $cm^2 \mu m^{-1} sr^{-1}$, respectively. The Angstrom exponents were assumed to be zero, and certain geographical regions, such as the Sargasso Sea, were assumed to be clear-water sites at all times. Under these assumptions, the clear-water L_{WN} values were used to calculate calibration adjustment coefficients to bring CZCS derived L_{WN} values into agreement for these regions. The vicarious calibration of the 443 nm band is tenuous, because of the great variability in $L_{WN}(443)$ even in clear water. Additionally, certain command and engineering data from the NIMBUS-7 platform were not archived, so that a detailed analysis of possible effects related to the spacecraft environment and the effects of spacecraft operation on the calibration could not be performed.

Unlike CZCS, SeaWiFS and other modern ocean color sensors routinely produce geophysical fields in a near-real time, operational mode for distribution to the science community. This aspect, as well as merger of multi-satellite data sets spanning many years, necessitates constant evaluation of system performance and derived products for all of the sensors. Therefore, a consistent multifaceted approach to address problems of sensitivity degradation and sensor characterization is required on a continuing basis. The goal is to ensure that satellite derived water-leaving radiances are accurately known and meet the specifications of the individual missions and SIMBIOS.

As implemented by the SeaWiFS Project Office, for example, the validation program includes both onboard and vicarious calibration approaches (McClain *et al.* 1998, 2000a, 2000b; Barnes *et al.* 1999a, 2000a, 2000b, 2000c). SeaWiFS has a solar measuring diffuser plate to reference the response to the sun and is also capable of periodically imaging the moon by maneuvering the spacecraft (Barnes *et al.* 1999b). MODIS and some other ocean color sensors have similar capabilities. The vicarious calibration program incorporates measurements of water-leaving radiances, and other related quantities, from ships, drifting buoys, and fixed moorings, to develop time series and geographically diverse samples of oceanic and atmospheric data. Each approach has advantages and disadvantages, but when combined, they should provide a complementary and comprehensive data set that will be sufficient to monitor short-term changes and long-term trends in the sensor's performance.

Presently, the SIMBIOS Project uses a combination of satellite and *in situ* observations from geographically diverse vicarious calibration test sites as a means of comparing ocean color satellite instruments. Using this vicarious calibration approach, results retrieved from different sensors can be meaningfully compared and possibly merged (Barnes *et al.* 2001). More importantly, one can use the same procedure, with *in situ* ocean and atmospheric optical property measurements, to recalibrate satellite sensors (Fargion *et al.*, 1999, 2000; Fargion and McClain 2000).

The SIMBIOS calibration strategy is to focus on regions and circumstances where the optical properties of the marine atmosphere and ocean are well understood and homogeneous, *i.e.* where the errors in the atmospheric correction and the *in situ* optical measurements are expected to be minimal. The Marine Optical Buoy (MOBY), near the island of Lanai, Hawaii, provides the principal instrumented test site for vicarious calibration measurements (Clark *et. al.* 1997; see also Volume VI, Chapter 2). The MOBY project officially supports the validation of ocean

color data that is collected by SeaWiFS and MODIS. In addition, MOBY has been successfully used for OCTS and POLDER and indirectly for MOS (Wang and Franz, 1999) vicarious calibrations.

1.4 BIO-OPTICAL ALGORITHMS

The SeaWiFS Project Office, and each of the counterpart ocean color sensor projects, is responsible for producing a standard set of derived products. The oceanic products include chlorophyll concentration, $K_d(490)$, and $L_{WN}(\lambda,\theta,\phi)$ at 5 wavelengths (see Volume III, Chapter 4 regarding the significance of the angular dependency).

The basic quantities to be computed from the sensor radiances are the water-leaving radiances, from which all other derived products except the aerosol products are computed. Every effort must be made to ensure these radiances meet the goal of no more than 5 % uncertainty in case-1 waters. This requires the atmospheric correction algorithms to be considerably more sophisticated than were the original CZCS algorithms.

The baseline bio-optical products must meet the SeaWiFS, MODIS, other sensors, and SIMBIOS Project accuracy requirements over a variety of water masses. The CZCS algorithms were based on a data set consisting of fewer than 50 data points (only 14 observations were available for the band-2-to-band-3 ratio algorithm) and performed poorly in regions of high concentrations of phytoplankton pigments, suspended sediment, or CDOM, and in coccolithophorid blooms (Groom and Holligan 1987). Accurate estimates of the baseline products are essential if SeaWiFS is to be useful in programs such as the Joint Global Ocean Flux Study (JGOFS) [National Academy of Science (NAS) 1984], carbon cycle research, and climate change research.

SeaWiFS, and the other modern ocean color sensors, have the capability, due to improvements in the signal-to-noise ratio (SNR), digitization, dynamic range, and wavelength selection, to increase the accuracy of these products and to flag areas where anomalies or low confidence conditions exist. Clearly, a much larger database is needed for developing and validating a broader variety of bio-optical algorithms, some of which will be region specific. The radiometric, optical, and chemical field observations used in deriving bio-optical algorithms and for vicarious calibration of the sensor must, therefore, conform to stringent, uniform requirements with respect to instrument calibration and characterization, and methods of observation.

The SeaWiFS and SIMBIOS Projects jointly manage a program to compare the various atmospheric correction and bio-optical algorithms proposed by the science community (Wang and Bailey 2000, McClain *et al.* 2000a, 2000b; O'Reilly *et al.* 2000). The purpose of this program is to independently evaluate suggested improvements, or additions, to the SeaWiFS and merged products. This component of the calibration and algorithm development program runs in parallel with, but off-line from, operational processing and provides an essential mechanism for incorporating data and analyses from the community at large (Barnes *et al.* 2001).

1.5 VICARIOUS CALIBRATION

For ocean observations, it is easy to show (Gordon 1987 and Gordon 1988) that satellite sensor calibration requirements based on the quality of the existing CZCS pigment algorithms exceed currently available capabilities. Furthermore, the sensor calibration is unlikely to remain unchanged through launch and five years of operation in orbit. The only foreseeable way of approaching the ocean calibration needs is through vicarious calibration, *i.e.*, fine tuning the calibration in orbit.

Gordon (1987) described the detailed method used to achieve vicarious calibration for the CZCS. First, the calibration was initialized after launch by forcing agreement between the sensor-determined radiance and the expected radiance based on radiometric measurements made at the surface under clear atmospheric conditions. Next, since the CZCS responsivity was observed to be time dependent, the algorithms were applied to other scenes characterized by bio-optical surface measurements and more typical atmospheres, and the calibration was adjusted until the measured water-leaving radiances were reproduced. Finally, the surface measurements of pigments were combined with satellite pigment estimates for a wide variety of atmospheric conditions, and the radiance calibration was fine tuned until the best agreement was obtained between the retrieved and true pigments.

The CZCS vicarious calibration was not radiometric. It was a calibration of the entire system - sensor plus algorithms. To predict the radiance measured at the satellite, L_t, the water-leaving radiance, aerosol optical

thickness, and aerosol phase function are all required. Also needed are ancillary data, including the surface pressure, wind speed, and ozone optical thickness. For vicarious calibration and validation, these data are obtained by measuring the upwelling radiance distribution just beneath the surface, along with the aerosol optical thickness and the sky radiance, at the time of the satellite overpass. The sky radiance is used to deduce the required information about the aerosol phase function (Voss and Zibordi 1989). The data set is finally used to deduce L_t, at the top of the atmosphere, coincident with a SeaWiFS overpass from which the calibration is initialized (Clark *et al.* 1997).

The present approach used by the SIMBIOS and SeaWiFS Projects is to develop a Level-1b to Level-2 software package (MSl12) which is capable of processing data from multiple ocean color sensors using the standard SeaWiFS atmospheric correction algorithms of Gordon and Wang (1994a, 1994b). The integration of a new sensor into MSl12 involves the development of a set of input functions and derivation of bandpass specific quantities such as Rayleigh scattering tables and Rayleigh-aerosol transmittance tables. Once the processing capability has been established, the vicarious calibration can be tuned using "match-up data" from the MOBY site, and/or cross calibration with another sensor. For example, Wang and Franz (1999) used SeaWiFS normalized remote sensing reflectances and aerosol models to successfully re-calibrate the MOS spectral channels.

Using this approach, the SIMBIOS Project can provide a completely independent assessment of instrument calibration and sensor-to-sensor relative calibration. The Project also provides insight to the sensor teams on how differences in calibration techniques and atmospheric correction algorithms propagate through the processing to produce differences in retrieved optical properties of the water. It must be stressed that this exercise is absolutely essential for calibrating the ocean color systems, *i.e.* sensors plus algorithms, and that it cannot be implemented without a high quality surface data set obtained simultaneously with the satellite imagery.

1.6 AEROSOL OPTICAL THICKNESS VALIDATION

Aerosol optical thickness products determined from the satellite ocean color data itself are critical factors in the uncertainty budgets of atmospheric correction algorithms (Gordon and Wang 1994a) and results of vicarious calibrations (Clark *et al.* 1997; Gordon 1981, 1987, 1988). The SIMBIOS Project is validating the SeaWiFS aerosol optical products by comparing them to *in situ* measurements (Wang *et al.*, 2000). A second, related objective of these comparisons is to determine the validity of the aerosol models currently used by SeaWiFS for atmospheric correction.

The principal source of *in situ* aerosol observations is the Aerosol Robotic Network (AERONET). AERONET is a network of ground-based automated sun photometers owned by national agencies and universities (Holben *et al.* 1998). AERONET data provides globally distributed, near-real time observations of aerosol spectral optical depths, aerosol size distributions, and precipitable water. Because the majority of the AERONET stations are at continental locations, SIMBIOS augmented the network with 12 additional island and coastal sites, including Lanai and Oahu Hawaii, Ascension Island, Bahrain, Tahiti, Wallops Island, South Korea, Turkey, Argentina, Azores and Perth. The SIMBIOS Project also has shipboard and hand-held sun photometers (MicroTops, PREDE, and SIMBAD) and an aerosol-profiling LIDAR system. These instruments are calibrated in collaboration with the AERONET Program at NASA Goddard Space Flight Center (GSFC) and loaned to investigators staging SIMBIOS sponsored research expeditions.

1.7 COMMUNITY PARTICIPATION

The SeaWiFS and SIMBIOS Project Offices rely on the oceanographic community to perform field research for atmospheric and bio-optical algorithm development, and for all of the *in situ* data collection for vicarious sensor calibration. The SIMBIOS Project sponsors a subset of these observations, but many projects sponsored by the NASA Research and Application Program, other government agencies and the international ocean color research community all make major contributions to the global multi-year effort.

The SIMBIOS Project has undertaken the challenge of coordinating the *in situ* observations contributed by these various programs, linking it to ocean color imagery from the international ensemble of satellite sensors, and making the overall data sets available to the ocean color research community (McClain and Fargion 1999a, 1999b). A workable strategy to meet those challenges first requires a clear definition of the observations, uncertainties, and data collection protocols associated with each type of activity. The purpose of this document is to clarify these requirements.

1.8 PROTOCOL DOCUMENT ORGANIZATION

Beginning with Revision 4, this document is organized into 7 volumes:

Volume I, the present volume, covers perspectives on ocean color research and validation (Chapter 1), fundamental definitions, terminology, relationships and conventions used throughout the protocol document (Chapter 2), requirements for specific *in situ* observations (Chapter 3), and general protocols for field measurements, metadata, logbooks, sampling strategies, and data archival (Chapter 4). Chapters 1 through 3 here and in Revision 3 (Mueller and Fargion 2002) are essentially the same, while Chapter 4 combines material from Chapter 9 (Revision 3) with a brief summary of SeaBASS policy and archival requirements (the detailed SeaBASS information in Chapter 18 and Appendix B of Revision 3 has been separated from the optics protocols).

Volume II reviews instrument performance characteristics required for *in situ* observations to support validation (Chapter 1), provides detailed instrument specifications and underlying rationale (Chapter 2), and specifies protocols for instrument calibration and characterization standards and methods (Chapters 3 through 5). Chapters 1 through 5 of Volume II correspond directly to Chapters 4 through 8 (Revision 3), respectively.

Volume III briefly reviews methods used in the field to make *in situ* radiometric measurements for ocean color validation, together with methods of analyzing the data (Chapter 1) and provides detailed measurement and data analysis protocols for in-water radiometric profiles (Chapter 2), above water measurements of remote sensing reflectance (Chapter 3), determinations of exact normalized water-leaving radiance (Chapter 4), and atmospheric radiometric measurements to determine aerosol optical thickness and sky radiance distributions (Chapter 5). Volume III, Chapter 1 is adapted from relevant portions of Chapter 9 (Revision 3). Volume III, Chapter 2 corresponds to Chapter 10 (Rev. 3), and Chapters 3 through 5 to Revision 3 Chapters 12 through 14, respectively. Aside from reorganization, there are no changes in the protocols presented in this volume.

Volume IV includes a chapter reviewing the scope of inherent optical properties (IOP) measurements (Chapter 1), followed by 4 chapters giving detailed calibration, measurement and analysis protolcols for the beam attenuation coefficient (Chapter 2), the volume absorption coefficient measured *in situ* (Chapter 3), laboratory measurements of the volume absorption coefficients from discrete filtered seawater samples (Chapter 4), and *in situ* measurements of the volume scattering function, including determinations of the backscattering coefficient (Chapter 5). Chapter 4 is slightly revised version of Chapter 15 (Rev. 3), while the remaining chapters of this volume are entirely new contributions to the ocean optics protocols.

Volume V, Chapter 1 briefly reviews biogeochemical and bio-optical measurements, and points to literature covering methods for measuring these variables; some of the material in this overview is drawn from Chapter 9 (Revision 3). Detailed protocols for HPLC measurement of phytoplankton pigment concentrations are given in Chapter 2, which differs from Chapter 16 (Rev. 3) only by its specification of a new solvent program. Chapter V-3 gives protocols for Fluorometric measurement of chlorophyll *a* concentration, and is not significantly changed from Chapter 17 (Rev. 3). New chapters covering protocols for measuring, Phycoerythrin concentrations, Particle Size Distribution (PSD) and Particulate Organic Carbon (POC) concentrations are likely future additions to this volume.

Volume VI gathers chapters covering more specialized topics in the ocean optics protocols. Chapter 1 introduces these special topics in the context of the overall protocols. Chapter 2 is a reformatted, but otherwise unchanged, version of Chapter 11 (Rev. 3) describing specialized protocols used for radiometric measurements associated with the Marine Optical Buoy (MOBY) ocean color vicarious calibration observatory. The remaining chapters are new in Rev. 4 and cover protocols for radiometric and bio-optical measurements from moored and drifting buoys (Chapter 3), ocean color measurements from aircraft (Chapter 4), and methods and results using LASER sources for stray-light characterization and correction of the MOBY spectrographs (Chapter 5). In the next few years, it is likely that most new additions to the protocols will appear as chapters added to this volume.

Volume VII collects appendices of useful information. Appendix A is an updated version of Appendix A (Rev. 3) summarizing characteristics of past, present and future satellite ocean color missions. Appendix B is the List of Acronyms used in the report and is an updated version of Appendix C (Rev. 3). Similarly, Appendix C, the list of Frequently Used Symbols, is an updated version of Appendix D (Rev. 3). The SeaBASS file format information given in Appendix B (Rev. 3) has been removed from the protocols and is promulgated separately by the SIMBIOS Project.

REFERENCES

Barnes, R. A., R. E. Eplee, F. S. Patt, and C. R. McClain 1999a: Changes in the radiometric sensitivity of SeaWiFS determined from lunar and solar-based Measurements. *Applied Optics*, **38**, 4649-4669.

Barnes, R.A., R.E. Eplee, Jr., S.F. Biggar, K.J. Thome, E.F. Zalewski, P.N. Slater, and A.W. Holmes 1999b: The SeaWiFS Solar Radiation-Based Calibration and the Transfer-to-Orbit Experiment. *NASA Tech. Memo. 1999--206892, Vol. 5*, S.B. Hooker and E.R. Firestone, Eds., NASA Goddard Space Flight Center, 28 pp.

Barnes, R.A., R.E. Eplee, Jr., W.D. Robinson, G.M. Schmidt, F.S. Patt, S.W. Bailey, M. Wang and C.R. McClain, 2000a: The calibration of SeaWiFS, *Proc. 2000 Conf on Characterization and Radiometric Calibration for Remote Sensing*, Logan, Utah, Sept. 19-21, 2000.

Barnes, R.A., R.E. Eplee, Jr., W.D. Robinson, G.M. Schmidt, F.S. Patt, S.W. Bailey, M. Wang and C.R. McClain, 2000b: The calibration of SeaWiFS on-orbit. In: *Earth Observing Systems V*. (W.L. Barnes, Ed.), Proc. SPIE Vol. **4135:** 281-293.

Barnes, R.A., R.E. Eplee, Jr., S.F. Biggar, K.J. Thome, E.F. Zalewski, P.N. Slater and A.W. Holmes, 2000c. SeaWiFS transfer-to-orbit experiment, *Appl. Opt*., **39:** 5620-5631.

Barnes, R.A., D.K. Clark, W.E. Esaias, G.S. Fargion, G. C. Feldman and C.R. McClain, 2001. Development of a consistent multi-sensor global ocean color time series. *Proc. International Workshop on Geo-Spatial Knowledge Processing for Natural Resource Management, 28-29 June 2001*, (A. Belward, E. Biinaghi, P.A. Brivio, G.A. Lanzaroni and G. Tosti, Eds.), Univ. of Insubria, Varese, Italy, pp 13-28.

Brown, O. B., and R. H. Evans 1985: Calibration of Advanced Very High Resolution Radiometer infrared observations. *J .Geophys. Res*., **90**, 11,667-11,677.

Clark, D. K., 1981: Phytoplankton pigment algorithms for the Nimbus-7 CZCS. *Oceanography from Space*, J.F.R. Gower Ed., Plenum Press, 227-238.

Clark, D.K., H.R. Gordon, K.J. Voss, Y. Ge, W. Broenkow, and C.C. Trees, 1997: Validation of atmospheric correction over oceans. *J. Geophys. Res*., **102,** 17,209-17217.

Esaias, W., G. Feldman, C.R. McClain, and J. Elrod, 1986: Satellite observations of oceanic primary productivity. *EOS, Trans. AGU*, **67**, 835--837.

Evans, R.H., and H.R. Gordon, 1994: Coastal zone color scanner system calibration: A retrospective examination. *J. Geophys. Res.,* **99**, 7,293--7,307.

Fargion G.S., C.R. McClain, H. Fukushima, J.M. Nicolas and R.A. Barnes, 1999: Ocean color instrument intercomparisons and cross-calibrations by the SIMBIOS Project. *SPIE* Vol. **3870**,397-403.

Fargion, G.S. and C.R. McClain, 2000: Three years of ocean color instrument intercomparisons and cross-calibrations by the SIMBIOS Project (1997-2000), In: *Remote Sensing of the Ocean and Sea Ice 2000* (C.R. Bostater, Jr. and R. Santoleri, Eds.), Proc. SPIE Vol. **4172**: pp44-55.

Fargion, G., C.R. McClain and R.A. Barnes, 2000: Ocean color instrument intercomparisons and cross-calibration by the SIMBIOS Project (1999-2000). In: *Earth Observing Systems V* (W.L. Barnes, Ed.), Proc. SPIE Vol. **4135**: 411-420.

Fargion, G.S. and J.L. Mueller, 2000: *Ocean Optics Protocols for Satellite Ocean Color Sensor Validation, Revision 2*, NASA TM 2001-209955, NASA Goddard Space Flight Center, Greenbelt, Maryland, 184 pp.

Feldman, G., N. Kuring, C. Ng, W. Esaias, C. McClain, J. Elrod, N. Maynard, D. Endres, R. Evans, J. Brown, S. Walsh, M. Carle, and G. Podesta, 1989: Ocean Color: Availability of the global data set. *EOS*, *Trans. AGU*, **70**, 634.

Groom, S.B., and P.M. Holligan, 1987: Remote sensing of coccolithophorid blooms. *Adv. Space Res*., **7**, 73--78.

Gordon, H.R. and D.K. Clark, 1981: Clear water radiance for atmospheric correction of coastal zone color scanner imagery. *Appl. Opt.,* **20**,4,175-4,180.

Gordon, H.R., 1981: Reduction of error introduced in the processing of coastal zone color scanner-type imagery resulting from sensor calibration and solar irradiance uncertainty. *Appl. Opt*., **20**, 207--210.

Gordon H.R., J.W. Brown, O.B. Brown, R.H. Evans, and D.K. Clark 1983: Nimbus-7 CZCS: Reduction of its radiometric sensitivity with time. *Appl.Opt*., **24**, 3,929-3,931.

Gordon H.R., 1987: Calibration requirements and methodology for remote sensors viewing the ocean in the visible. *Remote Sens. Environ*.,**22**,103-126

Gordon H.R., 1988: Ocean color remote sensing systems: radiometric requirements. *Recent Advances in Sensors, Radiometry, and Data Processing for Remote Sensing*, P.N. Slater, Ed. SPIE, **924**, 151-157.

Gordon, H.R. and M. Wang, 1994a: Retrieval of water-leaving radiance and aerosol optical thickness over the oceans with SeaWiFS: A preliminary algorithm, *Appl. Opt*., **33**, 443-452.

Gordon, H.R. and M. Wang, 1994b: Influence of oceanic whitecaps on atmospheric correction of ocean color sensors, *Appl. Opt*., **33**, 7,754-7,763.

Holben, B.N., T.F. Eck, I. Slutsker, D. Tanre, J.P. Buis, A. Setzer, E. Vermote, J.A. Reagan, Y.J. Kaufman, T. Nakajima, F. Leaven, I. Jankowiak, and A. Smirnov, 1998: AERONET – a federated instrument network and data archive for aerosol characterization. *Remote Sens. Environ*., **66**, 1-16.

Hovis W.A., J.S. Knoll, and G.R. Smith, 1985: Aircraft measurements for calibration of a orbiting spacecraft sensor. *Appl.Opt.,* **24**,407-410.

McClain, C.R., W.E. Esaias, W. Barnes, B. Guenther, D. Endres, S. Hooker, G. Mitchell and R. Barnes, 1992: Calibration and Validation Plan for SeaWiFS. *NASA Tech. Memo. 104566, Vol. **3**,* S.B. Hooker and E.R. Firestone, Eds., NASA Goddard Space Flight Center, Greenbelt, Maryland, 41pp.

McClain, C.R., G. Feldman and W.E. Esaias, 1993: Biological Oceanic Productivity, in *Atlas of Satellite Observations Related to Global Change*, R.Gurney, J.L.Foster (Eds.), Cambridge Press, NY, 251-263, 470 pp.

McClain, C.R., M. Cleave, G. Feldman, W. Gregg and S.B. Hooker, 1998: Science quality SeaWiFS Data for global biosphere research. *Sea Technology*, **39**, 10-16.

McClain, C.R. and G.S. Fargion, 1999a: SIMBIOS Project 1998 Annual Report, *NASA Tech. Memo. 1999-208645*, NASA Goddard Space Flight Center, Greenbelt, Maryland, 105 pp.

McClain, C.R. and G.S. Fargion, 1999b: SIMBIOS Project 1999 Annual Report, *NASA Tech. Memo. 1999-209486,* NASA Goddard Space Flight Center, Greenbelt, Maryland, 128 pp.

McClain C.R., E. Ainsworth, R. Barnes, R. Eppley et al., 2000a: SeaWiFS Postlaunch Calibration and Validation Part 1, *NASA TM 2000-206892, Vol. **9**, NASA Tech. Memo. 104566,* S.B. Hooker and E.R. Firestone, Eds., NASA Goddard Space flight center, Greenbelt, Maryland (in press).

McClain C.R., R. A. Barnes, R. E. Eplee, Jr., B. A. Franz, et al., 2000b: SeaWiFS Postlaunch Calibration and Validation Part 2, *NASA TM 2000-206892, Vol. **10**, NASA Tech. Memo. 104566,* S.B. Hooker and E.R. Firestone, Eds., NASA Goddard Space flight center, Greenbelt, Maryland (in press).

Morel and Gentili, 1996: Diffuse reflectance of oceanic waters. III. Implication of bidirectionality for the remote sensing problem, *Appl. Opt*., **35**, 4,850-4,862.

Mueller, J.L. 1985: Nimbus-7 CZCS: electronic overshoot due to cloud reflectance. *Appl. Opt.,* **27**,438-440.

Mueller, J.L. and R.W. Austin, 1992: Ocean Optics Protocols for SeaWiFS Validation. *NASA Tech. Memo. 104566, Vol. 5,* S.B. Hooker and E.R. Firestone, Eds., NASA Goddard Space flight center, Greenbelt, Maryland, 45 pp.

Mueller, J.L. and R.W. Austin, 1995: Ocean Optics Protocols for SeaWiFS Validation, Revision 1. *NASA Tech. Memo. 104566, Vol. **25**,* S.B. Hooker and E.R. Firestone, Eds., NASA Goddard Space flight center, Greenbelt, Maryland, 66 pp.

Mueller, J.L. and G.S. Fargion [Eds.], 2002: Ocean Optics Protocols for SeaWiFS Validation, Revision 3. *NASA Tech. Memo. 2002–210004*, NASA Goddard Space flight center, Greenbelt, Maryland, 308 pp.

O'Reilly J. E., S. Maritorena, D. Siegel et al., 2000 SeaWiFS Postlaunch Calibration and Validation Part 3, *NASA TM 2000-206892, Vol. 11, NASA Tech. Memo. 104566,* S.B. Hooker and E.R. Firestone, Eds., NASA Goddard Space flight center, Greenbelt, Maryland (in press).

UNESCO, 1994: Protocols for the Joint Global Ocean Flux Study (JGOFS) Core Measurements, *Manual and Guides 29*, 170pp.

Viollier, M., 1982: Radiance calibration of the Coastal Zone Color Scanner: a proposed adjustment. *Appl. Opt*., **21**, 1,142--1,145.

Voss, K. J. and G. Zibordi, 1989: Radiometric and geometric calibration of a spectral electro-optic "fisheye' camera radiance distribution system. *J. Atmos. Ocean. Tech*.., **6**, 652-662.

Wang, M. and B.A. Franz, 1999: Comparing the ocean color measurements between MOS and SeaWiFS. *IEEE Trans. Geosci. Remote Sens.*, in press.

Wang, M., S. Bailey, C. Pietras and C. R. McClain, 2000: Correction of Sun Glint Contamination on the SeaWiFS Aerosol Optical Thickness Retrievals, in McClain et al., SeaWiFS Postlaunch Calibration and Validation Analyses, Part 1*, NASA TM 2000-206892, Vol. 9*, in press.

Weinreb, M.P., G. Hamilton, S. Brown, and R.J. Koczor, 1990: Nonlinear corrections in calibration of Advanced Very High Resolution Radiometer infrared channels. *J. Geophys. Res*., **95**, 7,381--7,388.

Chapter 2

Fundamental Definitions, Relationships and Conventions

James L. Mueller[1] and Andre Morel[2]

[1]*Center for Hydro-Optics and Remote Sensing, San Diego State University, California*
[2]*Laboratoire d'Oceanographie, Universite Pierre et Marie Curie, France*

2.1 INTRODUCTION

The fundamental radiometric and optical quantities, physical relationships, terminology, and conventions underlying ocean color science are drawn from an extensive and growing literature. The present *Ocean Optics Protocols for Satellite Ocean Color Sensor Validation* document and its predecessors (Mueller and Fargion 2002; Fargion and Mueller 2000; Mueller and Austin 1992, 1995) are attempts to distill a uniform set of concepts, methods and conventions applied to *in situ* measurements, data analyses and interpretations appropriate for validating the operational performance and derived products associated with satellite ocean color sensors. Basic ocean optical and radiative transfer concepts, definitions and terminology used throughout the protocols are adapted from, *e.g.*, Preisendorfer (1960, 1976), Jerlov (1976), Morel and Smith (1982), more recent literature cited extensively in the individual chapters, and workshop discussions associated with the successive revisions of the document. Comprehensive treatments of radiative transfer concepts and methods relevant to ocean color are provided by, *e.g.*, Mobley (1994) and Preisendorfer (1976). Choices of particular published scales for, *e.g.*, mean extraterrestrial solar spectral irradiance and the spectral absorption and scattering spectra of pure water, originate with usage in the Nimbus-7 Coast Zone Color Scanner and SeaWiFS programs, recent literature, and working group discussions specifically related to the protocols; these scale conventions are expected to continue to evolve (*e.g.* Section 2.8 below).

The purpose of the present chapter is to present a succinct summary of the key definitions, relationships, conventions and terminology currently adopted for use throughout the protocol document. In the earlier revisions (Mueller and Fargion 2001; Mueller and Austin 1992, 1995), uniform usage in these areas was maintained by carefully editing each new, or significantly revised, chapter. As the scope and breadth of chapter authorship has expanded, authors new to the protocols have introduced variant terminology and conventions that pose an increasingly burdensome editorial task. It is hoped that by collecting the most common aspects of this topic in one place as a source guide for authors and co-authors of protocol chapters, a more uniform usage and terminology may result. As with all chapters of the protocols, it is fully expected that, in the future, this first attempt will be significantly revised and improved through constructive criticism and suggestions from the ocean color research community at large.

The present chapter does not address important fundamental quantities, concepts and relationships of atmospheric optics, as they relate to ocean color science. A new section has been added to briefly define optical thickness, as this quantity is an important *in situ* atmospheric optical measurement for which protocols are described in Volume II, Chapter 4 and Volume III, Chapter 5. A comprehensive treatment of atmospheric optics is deferred, however, to a future revision to these protocols.

2.2 GEOMETRY

Remote Sensing Coordinate System

Figure 2.1 illustrates an arbitrary Cartesian coordinate system, with a source illuminating the origin from direction $\hat{\mathbf{S}}$, a unit-length vector oriented at (zenith, azimuth) angles (θ_o, ϕ_o), and a detector viewing the origin from direction $\hat{\mathbf{D}}$ oriented at (θ, ϕ). The orthonormal basis vectors $(\hat{\mathbf{x}}, \hat{\mathbf{y}}, \hat{\mathbf{z}})$, defined in matrix notation as

$$\hat{\mathbf{x}} = \begin{bmatrix} 1 \\ 0 \\ 0 \end{bmatrix}, \hat{\mathbf{y}} = \begin{bmatrix} 0 \\ 1 \\ 0 \end{bmatrix} \text{ and } \hat{\mathbf{z}} = \begin{bmatrix} 0 \\ 0 \\ 1 \end{bmatrix}, \tag{2.1}$$

define the coordinate system illustrated in Figure 2.1. The Cartesian representation of the unit-length vector pointing toward the detector is

$$\hat{\mathbf{D}} = \begin{bmatrix} \sin\theta\cos\phi \\ \sin\theta\sin\phi \\ \cos\theta \end{bmatrix}, \tag{2.2}$$

and the source direction vector coordinates are

$$\hat{\mathbf{S}} = \begin{bmatrix} \sin\theta_o\cos\phi_o \\ \sin\theta_o\sin\phi_o \\ \cos\theta_o \end{bmatrix}. \tag{2.3}$$

Photon flux from the source is transmitted through the origin in direction

$$\hat{\mathbf{T}} = -\hat{\mathbf{S}} = \begin{bmatrix} -\sin\theta_o\cos\phi_o \\ -\sin\theta_o\sin\phi_o \\ -\cos\theta_o \end{bmatrix}. \tag{2.4}$$

The scattering angle Ψ, through which photons are redirected from direction $\hat{\mathbf{T}}$ into direction $\hat{\mathbf{D}}$, in the view of the detector, is determined as $\cos\Psi = \hat{\mathbf{T}} \bullet \hat{\mathbf{D}}$, which from (2.2) and (2.4) expands in this coordinate frame as

$$\cos\Psi = -\cos\theta\cos\theta_o - \sin\theta\sin\theta_o\left(\cos\phi\cos\phi_o + \sin\phi\sin\phi_o\right).$$

Invoking the identity $\cos\left(\phi - \phi_o\right) = \cos\phi\cos\phi_o + \sin\phi\sin\phi_o$, the scattering angle in the remote sensing coordinate system may be expressed

$$\cos\Psi = -\cos\theta\cos\theta_o - \sin\theta\sin\theta_o\cos\left(\phi - \phi_o\right). \tag{2.5}$$

The complete derivation of (2.5), although straightforward, is given here because the sign of the second term has been incorrectly reversed in some literature sources (*e.g*. Gordon *et al*. 1983 and Liou 1980).

In the context of ocean color remote sensing, the $\hat{\mathbf{x}}\hat{\mathbf{y}}$-plane would be parallel to, and $\hat{\mathbf{z}}$ the unit normal to, the sea surface, the source would be the sun, and the detector a satellite ocean color sensor. A common convention appearing throughout this protocol document (*e.g*. see Volume III, Chapters 3 and 4) is to rotate the local coordinates so that the *x*-axis is aligned with the solar azimuth and $\phi_o \equiv 0$.

Instrument Coordinate System

When working with instruments designed to measure transmission of light along a path, or light scattered at a particular angle from that path, it is more convenient to rotate the coordinate system as illustrated in Figure 2.2. The collimated source is placed at $-\hat{\mathbf{z}}$ and "Detector 1" at $\hat{\mathbf{z}}$ to measure transmission of flux transmitted along that axis over the distance between source and sensor. "Detector 2" views the beam at the origin and zenith angle θ, and the associated scattering angle in this coordinate frame is simply $\Psi = \theta$. In ocean optics, it may ordinarily be assumed that scattering is azimuthally isotropic in the coordinate reference of Fig. 2, so that one need not consider ϕ dependence of scattering.

Scattering Angle Invariance

It is important to keep in mind that the relationship of the scattering angle Ψ to the angular orientation of the scattered (viewing) path relative to the transmission path is identical in Figures 2.1 and 2.2. Determining Ψ is simpler and more intuitive in the representation of Figure 2.2, when the origin and orientation of the transmission path are held fixed, and only the direction from which the origin is viewed varies. For a satellite remotely sensed ocean color image, on the other hand, both the source (transmission) and sensor (viewing) directions change continuously from pixel to pixel, and it is more convenient to place the origin at each pixel (Figure 2.1) and determine Ψ using (2.5).

Plane and Solid Angles

In plane geometry, quantities are represented in 2-dimensional Cartesian (x, y), or polar (r, θ), coordinates. The natural measure of angular distance in plane coordinates is the ***radian***, defined as the angle subtending an arc of unit length on the perimeter of the *unit circle* (*i.e.* a circle of radius $r = 1$). There are 2π radians in a full circle. The units of an angle are, by convention, taken implicitly to be radians (without units notation), unless they are explicitly specified to be in degrees. These simple definitions and concepts are widely understood and used by the public at large.

Radiometry and optics intrinsically involve vector quantities that must be represented in 3-dimensional (x, y, z), or (r, θ, ϕ), coordinates (Figure 2.1). It is also necessary to associate 3-dimensional ***solid angles*** with many radiometric and optical quantities. Following the definition of the 2-dimensional radian, the natural measure of solid angles in 3-dimensions is the ***steradian*** (denoted **sr**), defined as the solid angle subtending a unit area on the surface of the *unit sphere* (again $r = 1$). The geometry relating surface area on the unit sphere to angles θ and ϕ is illustrated in Figure 2.3. The differential area on the surface of a sphere of radius r is determined as $da = r^2 \sin\theta d\theta d\phi$, and on the unit sphere $da = \sin\theta d\theta d\phi$ (Figure 2.3). By definition, a given solid angle Ω corresponding to angular intervals $\Delta\theta$ and $\Delta\phi$ is determined as

$$\Omega = \int_{\Delta\phi}\int_{\Delta\theta} \sin\theta d\theta d\phi, \text{ sr}, \tag{2.6}$$

from which we define the differential solid angle as

$$d\omega \equiv \sin\theta d\theta d\phi, \text{ sr}. \tag{2.7}$$

2.3 IRRADIANCE AND RADIANCE

Taking radiant flux Φ to be the flow of radiant energy, e.g. in μW, through a point on a plane surface, ***irradiance*** is defined as $E \equiv \frac{d\Phi}{da}$, μW cm^{-2}, the radiant flux per unit area through that point from all directions in the hemisphere above the surface. The direction associated with E is the normal to the surface. ***Radiance*** at a point on a surface is the radiant flux per unit solid angle from direction (θ, ϕ), per unit area, $da\cos\theta$, normal to the direction of flow, and is defined as $L(\theta,\phi) \equiv \frac{d^2\Phi}{d\omega da\cos\theta} = \frac{dE}{\cos\theta d\omega}$, μW cm^{-2}sr^{-1}. Combining these definitions and (2.7) we have the relationship between irradiance and radiance incident on a plane as

$$E = \int_0^{2\pi}\int_0^{\frac{\pi}{2}} L(\theta,\phi)\cos\theta\sin\theta d\theta d\phi, \ \mu\text{W cm}^{-2}. \tag{2.8}$$

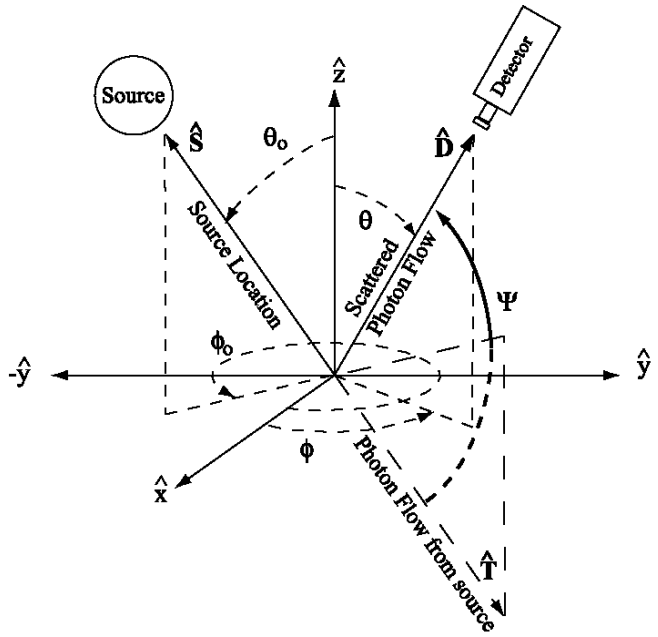

Figure 2.1: The directions of source $\hat{\mathbf{S}}$ and detector $\hat{\mathbf{D}}$ direction vectors relative to the origin of the coordinate frame adopted throughout the ocean optics protocols. The zenith and azimuth angles (θ_o, ϕ_o) are reserved for source directions, and the notation (θ, ϕ) applies to the direction of the detector location, or any other general direction, depending on the context. The unit-length vector $\hat{\mathbf{T}} = -\hat{\mathbf{S}}$ defines the direction of radiant flux from the source transmitted through the origin, and Ψ is the angle through which radiant flux is scattered from the transmitted beam $\hat{\mathbf{T}}$ into the view of the detector in direction $\hat{\mathbf{D}}$.

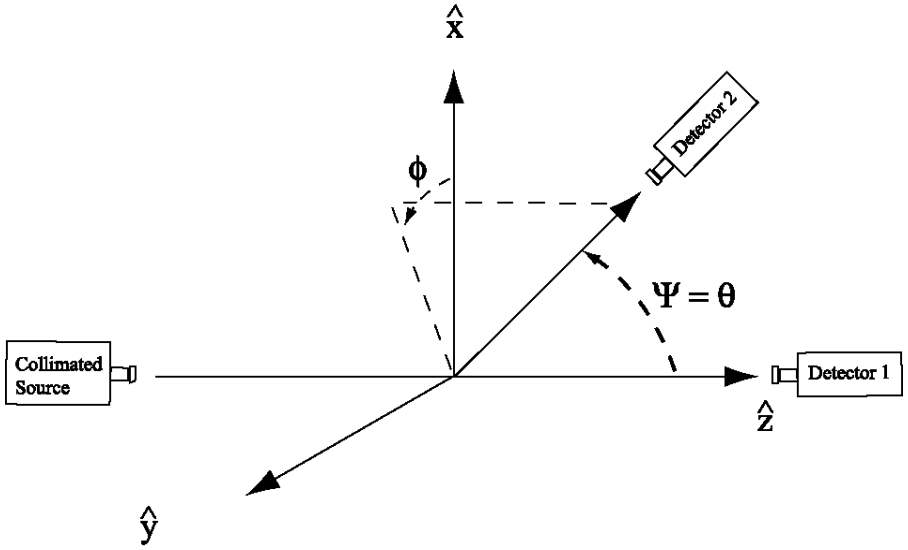

Figure 2.2: A local coordinate frame rotated to align the source and detector-1 locations along the z-axis. Detector-2, located in direction (θ, ϕ), views the origin to measure radiant flux scattered from the transmitted beam through angle Ψ. This local coordinate system is usually adopted for beam transmissometers and instruments designed to measure the volume scattering function (VSF) $\beta(\lambda, \Psi)$, because the scattering angle Ψ is more easily visualized and computed in this framework than in the representation of Figure 2.1. For a beam transmissometer, the path length is simply the distance between the source and detector-1 along the z-axis. For a VSF meter, the working volume is defined by the intersection of the field of view of detector-1 with the beam geometry of the source.

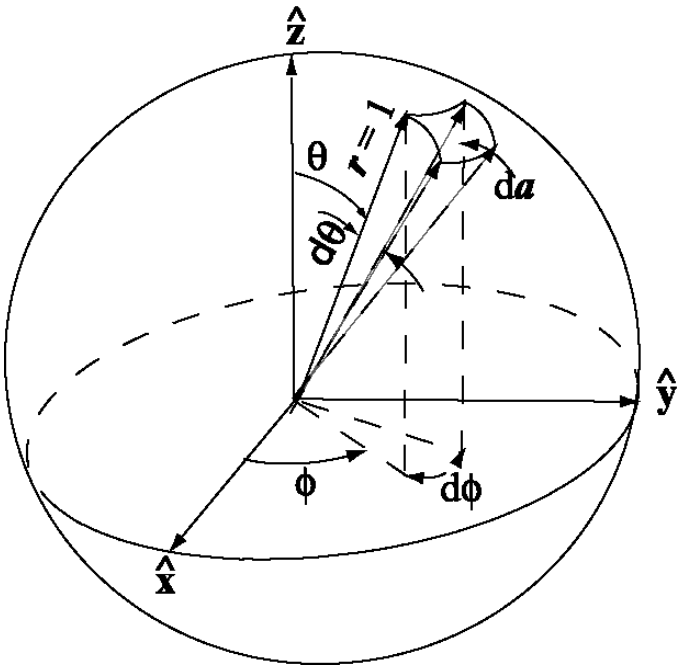

Figure 2.3: Illustration representing the relationship between differential angles $d\theta$ and $d\phi$ and the area da subtended on a sphere of unit radius. From the above, it is easily seen that $da = \sin\theta d\theta d\phi$.

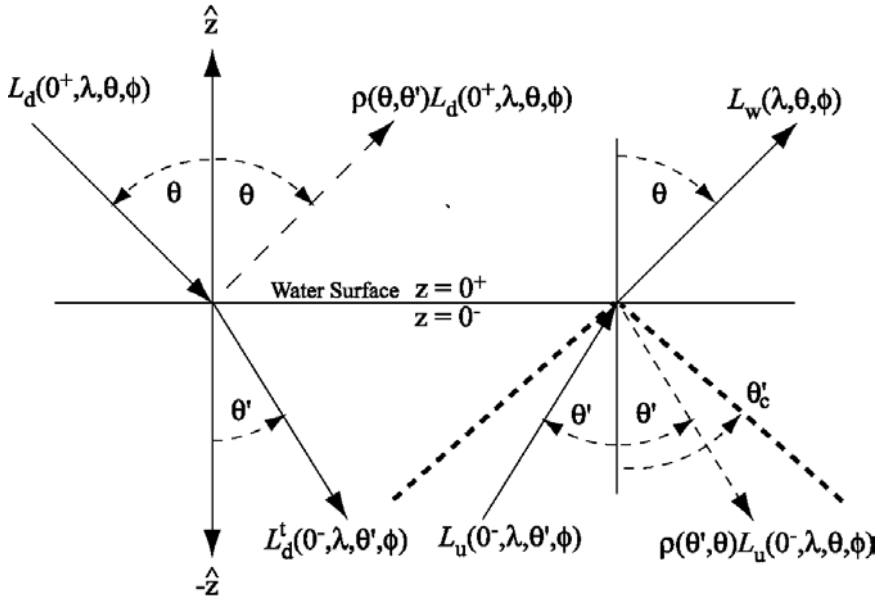

Figure 2.4: Reflection and refraction angles - in the plane of the paper - at the air-sea interface. Solid arrows represent radiant flux directions incident on and transmitted through the interface. Dashed arrows represent radiant flux reflected from the interface. The bold dashed lines represent the boundaries, in water, of the cone defined by the critical angle $\theta_c \approx 48^\circ$, beyond which radiant flux is totally reflected downward into the medium. The left-hand diagram represents the case for radiant flux incident from above $\left(z = 0^+\right)$ on, and reflected from, the surface at zenith angle θ, and transmitted through the interface at the refracted nadir angle θ' below the surface. The right-hand diagram represents the case for radiant flux incident from below $\left(z = 0^-\right)$ on, and reflected from, the surface at nadir angle θ', and transmitted through the interface at zenith angle θ in air. The symbols θ for zenith angles in air, and θ' for nadir angles in water, are adopted and reserved for this purpose throughout the ocean optics protocol document.

Irradiance and *radiance*, unless qualified as ***spectral*** quantities, include the flux of photons at all wavelengths.

Spectral irradiance is defined as $E(\lambda) \equiv \frac{d\Phi}{d\lambda}$, $\mu W\ cm^{-2} nm^{-1}$, and ***spectral radiance*** as $L(\lambda,\theta,\phi) \equiv \frac{dL(\theta,\phi)}{d\lambda}$, $\mu W\ cm^{-2} nm^{-1} sr^{-1}$, so from (2.8) we have for ***downward spectral irradiance*** incident on a plane surface from above

$$E_d(\lambda) = \int_0^{2\pi}\int_0^{\frac{\pi}{2}} L(\lambda,\theta,\phi)\cos\theta\sin\theta d\theta d\phi,\ \mu W\ cm^{-2} nm^{-1}, \tag{2.9}$$

and for ***upward spectral irradiance*** incident on the xy-plane from below (Figure 2.1)

$$E_u(\lambda) = -\int_0^{2\pi}\int_{\frac{\pi}{2}}^{\pi} L(\lambda,\theta,\phi)\cos\theta\sin\theta d\theta d\phi,\ \mu W\ cm^{-2} nm^{-1}. \tag{2.10}$$

Vector spectral irradiance, the net vertical radiant flux per unit area through a point from above and below the xy-plane[1], is by definition

$$\vec{E}(\lambda) = \int_0^{2\pi}\int_0^{\pi} L(\lambda,\theta,\phi)\cos\theta\sin\theta d\theta d\phi,\ \mu W\ cm^{-2} nm^{-1}, \tag{2.11}$$

or by inspection of (2.9) and (2.10), it is apparent that

$$\vec{E}(\lambda) = E_d(\lambda) - E_u(\lambda),\ \mu W\ cm^{-2} nm^{-1}. \tag{2.12}$$

Spectral scalar irradiance is the total flux of photons at wavelength λ per unit area (normal to the flux direction) from all directions through a point in space, or

$$\overset{o}{E}(\lambda) = \int_0^{2\pi}\int_0^{\pi} L(\lambda,\theta,\phi)\sin\theta d\theta d\phi,\ \mu W\ cm^{-2} nm^{-1}. \tag{2.13}$$

If an opaque surface of infinite extent is present at the xy-plane, as might be emulated with an instrument having a small spherical diffuser atop an opaque circular plate blocking flux from the lower hemisphere, the total flux through a point is the ***downward spectral scalar irradiance***

$$\overset{o}{E}_d(\lambda) = \int_0^{2\pi}\int_0^{\frac{\pi}{2}} L(\lambda,\theta,\phi)\sin\theta d\theta d\phi,\ \mu W\ cm^{-2} nm^{-1}, \tag{2.14}$$

and conversely for the underside of the xy-plane the ***upward spectral scalar irradiance*** is

$$\overset{o}{E}_u(\lambda) = \int_0^{2\pi}\int_{\frac{\pi}{2}}^{\pi} L(\lambda,\theta,\phi)\sin\theta d\theta d\phi,\ \mu W\ cm^{-2} nm^{-1}, \tag{2.15}$$

and in this case $\overset{o}{E}(\lambda) = \overset{o}{E}_d(\lambda) + \overset{o}{E}_u(\lambda)$.

The symbol $\overline{F}_o(\lambda)$ is traditionally used in atmospheric optics to describe the ***solar spectral irradiance above the earth's atmosphere*** on a plane normal to the direction of the sun, and when the earth is at its mean distance from the sun. The symbol $\overline{F}_o(\lambda)$ is kept in these protocols, for consistency with the literature providing scales of its values (Section 2.9 below), even though it represents irradiance and should otherwise be denoted using the symbol $E(\lambda)$.

[1] This is actually only the vertical component of vector spectral irradiance (Preisendorfer 1964, 1976; Mobley 1994), but the distinction is commonly omitted in the ocean optics literature.

2.4 INHERENT OPTICAL PROPERTIES OF SEAWATER

The ***inherent optical properties*** **(IOP)** of a medium, a term originating with Preisendorfer (1960), are quantities characterizing how a light field propagating through a given point in the medium is modified by the physical processes of absorption and scattering. The IOP are material properties of the medium, and they are independent of the geometric properties of the vector light field.

In contrast to the IOP, measurements of spectral irradiance and radiance propagating through a medium are dependent on the geometric distribution of the light field, as well as on the IOP of the medium. Under varying illumination conditions, such as variations in solar azimuth and zenith angle, these ***apparent optical properties*** **(AOP)** will vary also. The AOP are measurements of the vector light field in the sea, as determined by the surface illumination boundary conditions (the part of the downward radiance field at depth $z = 0^-$ that is transmitted through the surface from above) and the IOP. The bidirectional character of the ocean's remote sensing reflectance, which results from interaction of surface boundary conditions and the IOP, is examined in detail in Volume III, Chapter 4.

Coefficients of Absorption, Scattering and Beam Attenuation

Consider a narrow collimated beam, of cross-sectional area Δa, of monochromatic spectral energy flux $\Phi_i(\lambda)$, μW nm^{-1}, incident normal to the xy-plane at the origin of Figure 2.2. As the flux is transmitted over a distance Δz along the z-axis[2], a fraction $A(\lambda) = \dfrac{\Phi_A(\lambda)}{\Phi_i(\lambda)}$ will interact with and be absorbed by water molecules, or particles, another fraction $B(\lambda) = \dfrac{\Phi_B(\lambda)}{\Phi_i(\lambda)}$ will be scattered out of the beam into other directions, and the remaining fraction $T(\lambda) = \dfrac{\Phi_T(\lambda)}{\Phi_i(\lambda)}$ will be transmitted through the volume $\Delta a \Delta z$ cm^{2}m. The dimensionless fractions $A(\lambda)$, $B(\lambda)$, and $T(\lambda)$ are, respectively, the spectral absorptance, spectral scatterance, and spectral transmittance of the medium (*e.g.*, Mobley 1994). If there are no other sources in the medium, $A(\lambda) + B(\lambda) + T(\lambda) = 1$, and in the limits $\Delta a \to 0$ and $\Delta z \to 0$, we may write

$$\lim_{\Delta a \to 0} \lim_{\Delta z \to 0} \left\{ \frac{\Phi_T(\lambda) - \Phi_i(\lambda)}{\Delta a \Delta z} = -\frac{A(\lambda) + B(\lambda)}{\Delta z} \frac{\Phi_i(\lambda)}{\Delta a} \right\}, \ \mu\text{W cm}^{-2}\text{nm}^{-1}\text{m}^{-1}. \tag{2.16}$$

Since by definition $E(\lambda) = \dfrac{\Phi(\lambda)}{\Delta a}$, (2.16) may be written in differential form in terms of incident spectral irradiance as

$$\frac{dE_i(\lambda)}{dz} = -\left[a(\lambda) + b(\lambda)\right] E_i(\lambda) = -c(\lambda) E_i(\lambda), \ \mu\text{W cm}^{-2}\text{nm}^{-1}\text{m}^{-1}, \tag{2.17}$$

where $a(\lambda)$ is the ***spectral volume absorption coefficient*** $a(\lambda) = \lim_{\Delta z \to 0} \dfrac{A(\lambda)}{\Delta z}$, m^{-1}, $b(\lambda)$ is the ***spectral volume scattering coefficient*** $b(\lambda) = \lim_{\Delta z \to 0} \dfrac{B(\lambda)}{\Delta z}$, m^{-1}, and $c(\lambda)$ is the ***spectral volume beam attenuation coefficient***,

$$c(\lambda) = a(\lambda) + b(\lambda), \ \text{m}^{-1}. \tag{2.18}$$

[2] In the present context, the variable *z* in Fig. 2.2 does not correspond to depth in the water column, as it does elsewhere throughout this document. In Fig. 2.2 and the introduction of IOP, the *z*-axis defines only the direction of the optical path of radiant flux transmitted from the collimated source to "detector 1", and the angular orientation of the coordinate frame in the medium is arbitrary and irrelevant.

The Volume Scattering Function

The directional scatterance $B(\lambda,\Psi,\phi) \equiv \frac{\Phi_S(\lambda,\Psi,\phi)}{\Phi_i(\lambda)}$ is the fraction of incident radiant flux scattered from the volume $\Delta a \Delta z$ into a solid angle increment $\Delta\Omega$ centered in direction (Ψ,ϕ). Recall that $\Psi = \theta$ in the coordinate frame of Figure 2.2. In ocean optics, it is usually assumed that scattering of unpolarized light is azimuthally symmetric about the beam, and therefore, it is independent of ϕ in the coordinate frame of Figure 2.2. Following the derivation described by Mobley (1994), the ***spectral volume scattering function*** **(VSF)** may be defined as

$$\beta(\lambda,\Psi) = \lim_{\Delta\Omega\to 0}\lim_{\Delta z\to 0}\left\{\frac{\Phi_S(\lambda,\Psi,\phi)}{\Phi_i(\lambda)\Delta\Omega\Delta z}\right\},\ \mathrm{sr^{-1}m^{-1}}. \tag{2.19}$$

The spectral radiant intensity $I_S(\lambda,\psi,\phi)$ scattered from a point into direction (Ψ,ϕ) - as might be calculated for scattering by spherical particles using Mie theory, for example - is $I_S(\lambda,\psi,\phi) = \lim_{\Delta\Omega\to 0}\frac{\Phi_S(\lambda,\psi,\phi)}{\Delta\Omega}$, $\mu\mathrm{W\ nm^{-1}sr^{-1}}$. With appropriate substitutions, therefore, the definition of the VSF (2.19) may be rewritten as (Mobley 1994)

$$\beta(\lambda,\Psi) = \lim_{\Delta a\to 0}\lim_{\Delta z\to 0}\left\{\frac{I_S(\lambda,\Psi,\phi)}{E_i(\lambda)\Delta a\Delta z}\right\},\ \mathrm{sr^{-1}m^{-1}}. \tag{2.20}$$

The volume scattering coefficient is related to the VSF as

$$b(\lambda) = 2\pi\int_0^\pi \beta(\lambda,\Psi)\sin\Psi d\Psi,\ \mathrm{m^{-1}}. \tag{2.21}$$

The non-dimensional ***volume scattering phase function***, characterizing the shape of the VSF, is defined as

$$\tilde{\beta}(\lambda,\Psi) \equiv \frac{\beta(\lambda,\Psi)}{b(\lambda)}. \tag{2.22}$$

The volume scattering phase function gives the probability that, if a photon is scattered at all it will be redirected through angle Ψ, while the volume scattering coefficient characterizes the strength of the scattering process per unit pathlength.

The Backscattering Coefficient

The fraction per unit pathlength of the incident radiant flux scattered in the backward direction, *i.e.* $\Psi > \frac{\pi}{2}$, is the ***volume backscattering coefficient***

$$b_b(\lambda) = 2\pi\int_{\frac{\pi}{2}}^\pi \beta(\lambda,\Psi)\sin\Psi d\Psi,\ \mathrm{m^{-1}}. \tag{2.23}$$

The normalized backscattering coefficient, giving the probability that a scattered photon will be scattered through an angle $\Psi > \frac{\pi}{2}$, is defined as

$$\tilde{b}_b(\lambda) \equiv \frac{b_b(\lambda)}{b(\lambda)}, \tag{2.24}$$

or by combining (2.22) and (2.23)

$$\tilde{b}_b(\lambda) = 2\pi\int_{\frac{\pi}{2}}^\pi \tilde{\beta}(\lambda,\Psi)\sin\Psi d\Psi,\ \mathrm{m^{-1}}. \tag{2.25}$$

The Single Scattering Albedo

The ***single scattering albedo***

$$\varpi(\lambda) \equiv \frac{b(\lambda)}{a(\lambda)+b(\lambda)}, \tag{2.26}$$

alternatively denoted as ω_o, parameterizes the relative contribution of scattering to total attenuation of light in the medium and is also called the *probability of photon survival*, for a photon that interacts with the medium.

Fluorescence and Raman Scattering

The IOP of seawater discussed above deal only with absorption and elastic scattering by molecules and particles. The radiant field in water also includes *inelastic scattering* contributions due to radiant energy absorbed by the medium at one wavelength, and emitted at a longer wavelength. The coefficients characterizing these internal sources of radiant energy are also IOP of the medium. Fluorescence emission by chlorophyll *a*, other phytoplankton pigments, and dissolved organic molecular compounds is one important inelastic scattering process in seawater (Volume III, Chapter 4). Raman scattering by water molecules is the other important inelastic scattering process in the sea (Volume III, Chapters 2 and 4).

Additive Property of Inherent Optical Properties

The IOP of natural seawater are a combination of IOP of pure water (molecular scattering and absorption), materials dissolved in seawater (also molecular scattering and absorption), and suspended particles (particle scattering and absorption). Therefore, each individual IOP may be expanded as the sum of contributions by each of these material components.

For absorption,

$$a(\lambda) = a_w(\lambda) + a_p(\lambda) + a_g(\lambda),\ \mathrm{m}^{-1}, \tag{2.27}$$

where a_W, a_P and a_G are the absorption coefficients of pure water, particles and dissolved organic materials, respectively.

It is usually assumed that molecular scattering by dissolved organic materials is indistinguishable from molecular scattering by water, so that the VSF expands as

$$\beta(\lambda) = \beta_w(\lambda) + \beta_p(\lambda),\ \mathrm{m}^{-1}, \tag{2.28}$$

where β_W and β_P are respectively the VSFs of water and particles. Given the expansion of the absorption coefficient and VSF, it is straightforward to determine the expansions of all other IOP by combining (2.27) and (2.28) with equations (2.18) through (2.26).

It is possible to further partition absorption and scattering coefficients to account for mixtures of different types of particles, or dissolved materials (see, *e.g.*, Volume IV, Chapter 4).

Inherent Optical Properties of Pure Water

For purposes of these protocols, the coefficients for molecular absorption by pure water $a_W(\lambda)\ \mathrm{m}^{-1}$, are adopted from Sogandares and Fry (1997) for wavelengths between 340 nm and 380 nm, Pope and Fry (1997) for wavelengths between 380 nm and 700 nm, and Smith and Baker (1981) for wavelengths between 700 nm and 800 nm.

The volume scattering coefficients of pure water, $b_W(\lambda)\ \mathrm{m}^{-1}$, are given by Morel (1974). The molecular (Rayleigh) scattering phase function is

$$\tilde{\beta}_w(\Psi) = \frac{3\left(1+\cos^2\Psi\right)}{16\pi}, \tag{2.29}$$

or more generally

$$\tilde{\beta}_w(\Psi) = \frac{3(1+\delta)\left(1+\frac{1-\delta}{1+\delta}\cos^2\Psi\right)}{8\pi(2+\delta)}, \tag{2.30}$$

where δ is the depolarization ratio, which has an average value $\overline{\delta} \approx 0.09$ (Morel 1974).

IOP and Radiant Field Relationships Distributed in a Medium

The foregoing IOP definitions and relationships, presented above via equations (2.16) through (2.26), are expressed in a local coordinate system (Figure 2.2) that provides a convenient framework for describing measurement concepts. To apply the IOP and these relationships to vector radiant fields in the atmosphere ocean system, it is necessary to take account of variations with location of the IOP and vector radiant fields throughout the medium. The local "instrument coordinates" of Figure 2.2 are not useful in this context, and it is more appropriate to express the IOP and radiant field relationships in the coordinate frame of Figure 2.1, where the xy-plane is parallel to the air-sea interface and the z-axis is fixed as the local vertical. In this more general framework, an optical transmission path vector (r,θ,ϕ) is not restricted to $(r,0,0)$, as in Figure 2.2 and the above IOP definitions, so that the incremental pathlength Δz appearing in (2.16) through (2.20) becomes $\Delta r \equiv \frac{\Delta z}{\cos\theta}$, where θ is the zenith angle in the direction of photon flow[3]. As discussed in Section 2.2, the scattering angle $\Psi \neq \theta$ in the more general coordinate frame of Figure 2.1, but must be determined using (2.5). Moreover, azimuthally symmetric scattering about a transmission beam, while still assumed, is no longer synonymous with ϕ - independence of scattering.

Unless stated otherwise, it is assumed throughout the protocols that horizontal variations in IOP are negligible compared to vertical variations, so that the spatial distributions of the primary IOP are expressed as $a(z,\lambda)$, $b(z,\lambda)$, $c(z,\lambda)$, and $\beta(z,\lambda,\Psi)$. This so-called "plane-parallel assumption" does not suggest that IOP do not vary with geographic position, but simply that horizontal variations are weak enough to be neglected in radiative transfer calculations related to the ocean color problem. It is recognized that this assumption may break down in Case-2 water masses, and other special circumstances, where 3-dimensional radiative transfer processes must be taken into account.

The incident spectral radiance distribution at the origin associated with a perfectly collimated source incident on the plane normal to $\hat{\mathbf{S}} = (r=1,\theta_o,\phi_o)$ (Figure 2.1) is related to the incident spectral irradiance $E_i(\lambda,\theta_o,\phi_o) = \int_0^{2\pi}\int_0^{\pi} L_i(\lambda,\theta,\phi)\cos(\theta-\theta_o)\delta(\theta-\theta_o)\delta(\phi-\phi_o)\sin\theta d\theta d\phi$, where the Dirac delta function $\delta(\theta-\theta_o)$ is

$$\delta(\theta-\theta_o) \equiv \begin{cases} 1, & \theta=\theta_o, \\ 0, & \text{otherwise}, \end{cases}$$

and similarly for $\delta(\phi-\phi_o)$, so that within the constraints of this construct $E_i(\lambda,\theta_o,\phi_o) = \lim_{\Delta\Omega\to 0} L_i(\lambda,\theta_o,\phi_o)\Delta\Omega$. Scattered radiance $L_S(\lambda,\theta,\phi) = \lim_{\Delta a\to 0}\frac{I_S(\lambda,\theta,\phi)}{\Delta a}$, μW cm^{-2}nm^{-1}sr^{-1}, *i.e.* radiance is radiant intensity per unit area (Mobley 1994). Using these relationships in differential form, and taking account of the depth dependence of IOP and coordinate transformations, equation (2.17) may be rewritten as

$$\begin{aligned} \frac{dE_i(z,\lambda,\theta_o,\phi_o)}{dz}\cos(\pi-\theta_o) &= -\left[a(z,\lambda)+b(z,\lambda)\right]E_i(z,\lambda,\theta_o,\phi_o) \\ &= -c(z,\lambda)E_i(z,\lambda,\theta_o,\phi_o),\ \mu\text{W cm}^{-2}\text{nm}^{-1}\text{m}^{-1}, \end{aligned} \tag{2.31}$$

and equation (2.20) as

[3] Note that for the source direction and transmission vector conventions of Figure 2.2, $\theta = \pi - \theta_o$, and $\cos\theta = -\cos\theta_o$.

$$\frac{d^2 L_S(z,\lambda,\theta,\phi)}{dz\,d\omega}\cos\theta = \beta(z,\lambda,\Psi)\,L_i(z,\lambda,\theta_o,\phi_o),$$

or for more general radiance distributions, the scattered radiance per unit pathlength is expressed as

$$\frac{dL_S(z,\lambda,\theta,\phi)}{dz}\cos\theta = \int_0^{2\pi}\int_0^{\pi}\beta(z,\lambda,\Psi)\,L_i(z,\lambda,\theta_o,\phi_o)\sin\theta_o\,d\theta_o\,d\phi_o,\ \mu W\ cm^{-2}nm^{-1}sr^{-1}m^{-1}. \qquad (2.32)$$

2.5 REFLECTION AND REFRACTION AT THE SEA SURFACE

The geometric aspects of reflection from, and refracted transmission through, the air-sea interface are illustrated in Figure 2.4. The water surface is located at depth z = 0, and the upper side of the interface is denoted $z = 0^+$, while the underside of the interface at the same depth is denoted $z = 0^-$. Ray paths indicating radiance incident on, or transmitted through, the interface are illustrated as solid arrows. Ray paths indicating radiance reflected from the interface are shown as dashed arrows.

The Refractive Index of a Medium

The complex refractive index of a medium is denoted $m(\lambda) = n(\lambda) + in'(\lambda)$. The real part of the refractive index, $n(\lambda)$, is the ratio of the speed of light in one medium relative to that in another. The imaginary part, $n'(\lambda)$, is directly related to the volume absorption coefficient $a(\lambda)$ of the medium. The complex refractive index is another IOP of seawater. The imaginary part of the refractive index is not utilized in the present version of the protocols, and further use of the term "*refractive index*" is taken to mean the real part $n(\lambda)$.

The refractive index of air is approximately independent of wavelength with value $n \approx 1$. The refractive index of water relative to air is approximately $n_w(\lambda) \cong 1.34$. Its wavelength dependence, while weak throughout the visible spectrum, may be computed for fresh water from the empirical relationship (Austin and Halikas 1976) as

$$n_w(\lambda) = 1.325147 + \frac{6.6096}{\lambda - 137.1924}. \qquad (2.33)$$

Austin and Halikas (1976) also tabulated variations in $n_w(\lambda)$ for seawater as a function of temperature and salinity; these variations are also weak, for visible wavelengths, and may be neglected for most applications discussed in these protocols.

Snell's Law of Refraction at a Plane Interface Between Two Media

Because the speed of light in seawater is approximately $\frac{3}{4}$ of that in air, radiance incident on the sea surface at angle θ is refracted to an angle θ' that is closer to the vertical (left-hand diagram in Figure 2.4). The reverse process takes place when upward radiance incident from below is transmitted across the interface into air (right-hand diagram of Figure 2.4). The angles θ and θ' are related by Snell's Law of Refraction

$$n = \frac{\sin\theta}{\sin\theta'}. \qquad (2.34)$$

Downward radiance from solid angle Ω sr in air that is transmitted through the interface, converges into a smaller solid angle Ω' sr in water. The reverse process, solid angle divergence, occurs when radiance is transmitted upward from water to air. By combining (2.6) with (2.34), it may be shown that the solid angles are related as $\Omega = n_w^2\Omega'$, where we neglect the weak wavelength dependence for wavelengths of interest in these protocols. There are two important consequences of the refractive radiance convergence/divergence relationship. The first is that downward radiance incident on the sea surface from the entire upper hemisphere converges in water into the cone defined by the critical angle $\theta_c' \cong 48.3°$, for $n_w \cong 1.34$, and conversely light transmitted upward as water-leaving radiance originates entirely within the critical angle cone. The second important consequence is that upward radiance incident on the sea surface from below at angles $\theta' > \theta_c'$ is totally reflected internally and contributes strongly to the downward radiance field at $z = 0^-$. The occurrence of total internal reflectance of upward radiance

beyond the critical angle explains why although approximately 97% of downward irradiance is transmitted through the interface into water, only about 52% of upward irradiance is transmitted through the interface into the air (see also Volume III, Chapter 4).

Reflection at the Sea Surface

Reflectance from a plane surface is determined by the Fresnel Reflectance function,

$$\rho_F(\theta,\theta') = \frac{1}{2}\left|\frac{\sin^2(\theta-\theta')}{\sin^2(\theta+\theta')} + \frac{\tan^2(\theta-\theta')}{\tan^2(\theta+\theta')}\right|, \tag{2.35}$$

where the first and second terms in vertical brackets are the reflectances for light components polarized, respectively, perpendicular and parallel to the plane of incidence. The plane of incidence as illustrated in Figure 2.1, for example, is the plane defined by the z-axis and the solar vector $\hat{\mathbf{S}}$. As above, the angles θ and θ' are the incidence angles in air and water, as related by (2.34), and the angle of reflection is equal to the angle of incidence, either above, or below the surface (Figure 2.4). An important property of (2.35) is that $\rho_F(\theta',\theta) = \rho_F(\theta,\theta')$, *i.e.* the reflectance for light incident from below at angle θ' and refracted on transmission to angle θ in air, is the same as reflectance for light incident from above at angle θ and refracted to angle θ' in water. When $\theta = \theta' = 0$, *i.e.* for normal incidence,

$$\rho_F(0,0) = \left[\frac{n-1}{n+1}\right]^2, \tag{2.36}$$

and for an air-water interface $\rho_F(0,0) \cong 0.02$.

Were the sea surface a flat plane, its reflectance $\rho(\theta',\theta;W) = \rho(\theta,\theta';W)$ would be simply the Fresnel reflectance as given in (2.35). However, wave roughness elements are always present on the sea surface, and its slope spectrum is related to wind speed W by the empirical relationship of Cox and Munk (1954). Even when $W = 0$, variation of surface tension induced by the passage of swell generates capillary waves to create a surface slope spectrum of small, but significant, amplitude. The Fresnel reflectance does hold locally for each tilted wave facet, so the reflectance of the sea surface $\rho(\theta,\theta';W)$ may be modeled by combining the Cox-Munk (1954) equations for the slope spectrum with (2.35) (Austin 1974; Morel and Gentili 1996; Mobley.1999). The determination and applications of $\rho(\theta,\theta';W)$ are discussed at more length in Volume III, Chapters 3 and 4, and in references cited in those chapters.

Radiance Transmittance Through the Sea Surface

With reference to Figure 2.4, the downward transmittance of radiance through the interface is given by

$$L_d^t(0^-,\lambda,\theta',\phi) = L_d(0^+,\lambda,\theta,\phi)n^2\left[1-\rho(\theta,\theta';W)\right], \tag{2.37}$$

and upward transmittance by

$$L_W(\lambda,\theta,\phi) = L_u(0^-,\lambda,\theta',\phi)\frac{\left[1-\rho(\theta',\theta;W)\right]}{n^2}, \tag{2.38}$$

where $L_W(\lambda,\theta,\phi)$ is ***water-leaving radiance***, which is defined only at $z = 0^+$ and the explicit depth notation is omitted.

2.6 THE RADIATIVE TRANSFER EQUATION

The propagation of radiance through the sea, assuming that IOP are horizontally homogeneous, is governed by the radiative transfer equation (RTE)

$$\frac{dL(z,\lambda,\theta',\phi)}{dz}\cos\theta' = -c(z,\lambda)L(z,\lambda,\theta',\phi) + \int_0^{2\pi}\int_0^{\pi}\beta(z,\lambda,\Psi)L(z,\lambda,\theta'_o,\phi_o)\sin\theta'_o d\theta'_o d\phi_o + L_r(z,\lambda) + L_F(z,\lambda),\ \mu W\ cm^{-2}nm^{-1}sr^{-1}m^{-1}, \quad (2.39)$$

where z is depth in m, $L_r(z,\lambda)$ and $L_F(z,\lambda)$ are, respectively, inelastic scattering radiance emissions (assumed to be isotropic) due to Raman scattering by water and fluorescence by particles and dissolved matter (see also Volume III, Chapters 2 and 4), and the other variables are previously defined. Angular relationships in (2.39) are as in Figure 2.1 and the scattering angle Ψ is related to angles (θ',ϕ) and (θ'_o,ϕ_o) by equation (2.5). The first term on the right-hand-side of (2.39) accounts for attenuation of radiance transmitted over path $\frac{dz}{\cos\theta'}$, and the second term represents the increase in radiance over that path due to photons scattered into direction (θ',ϕ) from all other (source) angles (θ'_o,ϕ_o) (Fig. 2.1). The combined radiance increase contributed by the three elastic and inelastic scattering source terms is called ***path radiance***, following Preisendorfer (1964).

The RTE, equation (2.39), is given here as a compact way to describe the basic relationship between the IOP and vector radiant fields in water. The reader interested in methods of solving the RTE for a given vertical distribution of IOP and surface boundary conditions, $L_d^t(0^-,\lambda,\theta',\phi)$ and $\rho(\theta,\theta';W)$, is referred to, *e.g.*, Mobley (1994) and references cited there. Solutions to the RTE figure prominently in the determination of exact normalized water-leaving radiance, as described in Volume III, Chapter 4.

The Beer-Lambert-Bouguer Law

In the absence of other sources, a collimated beam of radiance $L(\lambda,\theta,\phi)$ transmitted through seawater at a depth z m is attenuated along path $|\Delta r(\theta',\phi)| = \left|\frac{\Delta z}{\cos\theta'}\right|$ as

$$\frac{dL(z,\lambda,\theta',\phi)}{dz}\cos\theta' = -c(z,\lambda)L(z,\lambda,\theta',\phi),\ \mu W\ cm^{-2}nm^{-1}sr^{-1}m^{-1}, \quad (2.40)$$

under the same assumptions leading to (2.39). The solution to (2.40) for transmission of radiance over a path of length Δr is

$$L(z+\Delta z,\lambda,\theta',\phi) = L(z,\lambda,\theta',\phi)e^{-\frac{1}{\cos\theta'}\int_{\Delta z}c(z,\lambda)dz},\ \mu W\ cm^{-2}nm^{-1}sr^{-1}. \quad (2.41)$$

Equation (2.41) is called the Beer-Lambert-Bouguer Law, and represents only the attenuation term in the RTE, (2.39).

The Beer-Lambert-Bouguer Law in the form of (2.41) is applicable only in a purely absorbing medium, or in a situation where a single source produces a narrow collimated beam that is transmitted to a detector over a distance short enough that multiple scattering path radiance is negligible (*e.g.* the source to detector-1 path of Figure 2.2). The latter case is the basis for determining $c(\lambda)$ using a beam transmissometer (Volume IV, Chapter 2).

2.7 RADIOMETRIC QUANTITIES IN OCEAN COLOR REMOTE SENSING

Radiance Fields at the Sea Surface in Water and Air

The boundary conditions for the radiative transfer formulation of the ocean color remote sensing problem are the downward radiance field $L_d^t(0^-,\lambda,\theta',\phi)$ and the wind-speed dependent reflectance $\rho(\theta,\theta';W)$. Equation (2.37) relates these boundary conditions to the incident downward radiance field $L_d(0^+,\lambda,\theta,\phi)$ above the surface.

The downward radiance field $L_d^t(0^-,\lambda,\theta',\phi)$ is transmitted into the medium, where it is absorbed and redistributed by scattering, as in (2.39), to produce the radiance fields $L_d(z,\lambda,\theta',\phi)$ and $L_u(z,\lambda,\theta',\phi)$. As illustrated in Figure 2.4, part of the upwelling radiance field $L_u(0^-,\lambda,\theta',\phi)$ is reflected downward at the interface (all of it for $\theta' > \theta'_c$), so that the total downward radiance field at $z = 0^-$ is

$$L_d(0^-,\lambda,\theta',\phi) = L_d^t(0^-,\lambda,\theta',\phi) + \rho(\theta',\theta;W)\,L_u(0^-,\lambda,\theta',\phi). \tag{2.42}$$

The upwelling radiance field in air at $z = 0^+$ is water leaving radiance, as given by (2.38), combined with the radiance field reflected upward at the surface, i.e.

$$L_u(0^+,\lambda,\theta,\phi) = L_W(\lambda,\theta,\phi) + \rho(\theta,\theta';W)\,L_d(0^+,\lambda,\theta,\phi). \tag{2.43}$$

Irradiance at the Sea Surface in Water and Air

The downward and upward irradiance in water and air at the interface are determined by integrating the vector radiance fields, using the general relationships (2.9) and (2.10) above, to determine ***downward spectral irradiance*** above the interface

$$E_d(0^+,\lambda) \equiv \int_0^{2\pi}\int_0^{\frac{\pi}{2}} L_d(0^+,\lambda,\theta,\phi)\cos\theta\sin\theta\,d\theta\,d\phi, \tag{2.44}$$

which is often denoted $E_S(\lambda) \equiv E_d(0^+,\lambda)$ throughout the protocol chapters, ***downwelled spectral irradiance*** just beneath the interface

$$E_d(0^-,\lambda) \equiv \int_0^{2\pi}\int_0^{\frac{\pi}{2}} L_d(0^-,\lambda,\theta',\phi)\cos\theta'\sin\theta'\,d\theta'\,d\phi, \tag{2.45}$$

upwelled spectral irradiance just beneath the interface

$$E_u(0^-,\lambda) \equiv \int_0^{2\pi}\int_0^{\frac{\pi}{2}} L_u(0^-,\lambda,\theta',\phi)\cos\theta'\sin\theta'\,d\theta\,d\phi, \text{ and} \tag{2.46}$$

and ***upwelled spectral irradiance*** just above the interface

$$E_u(0^+,\lambda) \equiv \int_0^{2\pi}\int_0^{\frac{\pi}{2}} L_u(0^+,\lambda,\theta,\phi)\cos\theta\sin\theta\,d\theta\,d\phi, \ \mu\text{W cm}^{-2}\text{nm}^{-1}. \tag{2.47}$$

It should be noted that because of the contributions of reflected radiance away from each side of the interface, as expressed in (2.42) and (2.43), one couldn't determine, *e.g.*, $E_d(0^-,\lambda)$ by simply transmitting $E_d(0^+,\lambda)$ downward across the interface.

Vertical Profiles of Irradiance and Radiance in Natural Waters

Given solutions to the RTE (2.39) for particular surface boundary conditions and IOP profiles within the water column, it is straightforward to substitute the depth variable z to extend equations (2.45) and (2.46) to define the profiles of downwelling and upwelling spectral irradiance $E_{\mathrm{d}}(z,\lambda)$ and $E_{\mathrm{u}}(z,\lambda)$, respectively. However, radiance distribution profiles $L_{\mathrm{d}}(z,\lambda,\theta',\phi)$ and $L_{\mathrm{u}}(z,\lambda,\theta',\phi)$ are not ordinarily measured as functions of depth, and so it is assumed that diffuse attenuation of $E_{\mathrm{d}}(z,\lambda)$ and $E_{\mathrm{u}}(z,\lambda)$ follows the form of the Beer-Lambert-Bouguer Law as

$$E_{\mathrm{d}}(z,\lambda) = E_{\mathrm{d}}(0^-,\lambda)e^{-\int_0^z K_{\mathrm{d}}(z,\lambda)dz}, \tag{2.48}$$

and

$$E_{\mathrm{u}}(z,\lambda) = E_{\mathrm{u}}(0^-,\lambda)e^{-\int_0^z K_{\mathrm{u}}(z,\lambda)dz}, \tag{2.49}$$

where $K_{\mathrm{d}}(z, \lambda)$ and $K_{\mathrm{u}}(z, \lambda)$ are the respective ***diffuse attenuation coefficients*** for downwelled and upwelled spectral irradiance. Methods for determining $K_{\mathrm{d}}(z, \lambda)$ and $K_{\mathrm{u}}(z, \lambda)$ from measured profiles of $E_{\mathrm{d}}(z,\lambda)$ and $E_{\mathrm{u}}(z,\lambda)$ are described in Volume III, Chapter 2.

It is also common to measure vertical profiles of nadir-viewing upwelled radiance $L_{\mathrm{u}}(z,\lambda) \equiv L_{\mathrm{u}}(z,\lambda,0,0)$. It is assumed that the vertical attenuation of upwelled radiance also follows the form of the Beer-Lambert-Bouguer Law as

$$L_{\mathrm{u}}(z,\lambda) = L_{\mathrm{u}}(0^-,\lambda)e^{-\int_0^z K_{\mathrm{L}}(z,\lambda)dz}, \tag{2.50}$$

where $K_{\mathrm{L}}(z, \lambda)$ is the diffuse attenuation coefficient for $L_{\mathrm{u}}(z,\lambda)$. Methods for determining $K_{\mathrm{L}}(z, \lambda)$ from measured profiles of $L_{\mathrm{u}}(z,\lambda)$, and for determining $L_{\mathrm{u}}(0^-,\lambda)$ by using (2.48) to extrapolate the measured $L_{\mathrm{u}}(z,\lambda)$ profile to the surface, are given in Volume III, Chapter 2.

Reflectance of Irradiance and Radiance in Natural Waters

Irradiance reflectance is defined as

$$R(z,\lambda) \equiv \frac{E_{\mathrm{u}}(z,\lambda)}{E_{\mathrm{d}}(z,\lambda)}. \tag{2.51}$$

Following Austin (1974) and Morel and Gentili (1996) the upwelled irradiance and radiance fields at $z = 0^-$ are related as

$$Q(0^-,\lambda,\theta',\phi) \equiv \frac{E_{\mathrm{u}}(0^-,\lambda)}{L_{\mathrm{u}}(0^-,\lambda,\theta',\phi)},\ \mathrm{sr}, \tag{2.52}$$

so that radiance reflectance may be determined in turn as

$$L_{\mathrm{u}}(0^-,\lambda,\theta',\phi) = \frac{E_{\mathrm{d}}(0^-,\lambda)R(0^-,\lambda)}{Q(0^-,\lambda,\theta',\phi)}. \tag{2.53}$$

Given $L_{\mathrm{u}}(0^-,\lambda,\theta',\phi)$, water-leaving radiance $L_{\mathrm{W}}(\lambda,\theta,\phi)$ may be determined from (2.38).

All of the quantities in (2.53), and therefore also $L_{\mathrm{W}}(\lambda,\theta,\phi)$, are AOP that are dependent on the surface boundary conditions and IOP of the water body. It is clear, therefore, that the remote sensing reflectance

$$R_{\mathrm{RS}}(\lambda,\theta,\phi)=\frac{L_{\mathrm{W}}(\lambda,\theta,\phi)}{E_{\mathrm{d}}(0^{+},\lambda)} \tag{2.54}$$

is also an AOP, and has a bidirectional nature that is dependent (in a first approximation) on solar zenith angle θ_o. In early attempts to account for this bidirectionality, Gordon and Clark (1981) assumed the factor Q to be a constant, following Austin (1974), and defined normalized water-leaving radiance $L_{\mathrm{WN}}(\lambda)$ as that radiance which would be observed if the sun were at zenith and at mean earth-sun distance and there were no atmosphere, i.e.

$$L_{\mathrm{WN}}(\lambda)=L_{\mathrm{W}}(\lambda,\theta,\phi)\frac{\overline{F}_{\mathrm{o}}(\lambda)}{E_{\mathrm{d}}(0^{+},\lambda)}, \tag{2.55}$$

where $\overline{F}_{\mathrm{o}}(\lambda)$ is the extraterrestrial solar spectral irradiance at mean earth-sun distance (Neckel and Labs 1984). Morel and Gentili (1991, 1993, 1996) demonstrated conclusively, however, that Q is not constant and that $L_{\mathrm{WN}}(\lambda)$ remains an AOP with dependence on IOP, solar zenith angle, and surface roughness conditions. They further showed that by properly relating $Q(0^{-},\lambda,\theta',\phi)$ and $R(0^{-},\lambda)$ to IOP and θ_o, and relating $E_{\mathrm{d}}(0^{-},\lambda)$ to $E_{\mathrm{d}}(0^{+},\lambda)$ for a given θ_o and $\rho(\theta',\theta;W)$, it is possible to transform $L_{\mathrm{WN}}(\lambda)$ into an exact normalized water-leaving radiance $L_{\mathrm{WN}}^{\mathrm{ex}}(\lambda)$ that has been properly adjusted to remove bidirectional reflectance effects. The reader is referred to Volume III, Chapter 4 for a detailed discussion relating reflectance to IOP and θ_o, and describing the physical processes and approximations that relate water-leaving radiance to exact normalized water-leaving radiance. This is a critical topic and protocol chapter, because $L_{\mathrm{WN}}^{\mathrm{ex}}(\lambda)$ is the only valid form of water-leaving radiance by which measurements from satellite ocean color sensors and *in situ* radiometers may be compared.

2.8 ATMOSPHERIC OPTICAL THICKNESS

The optical properties of the atmosphere, as they affect transmission and reflection of spectral radiance between the top of the atmosphere (TOA) and sea surface, are critically important elements of ocean color science. The scope of the present protocols is limited, however, to *in situ* measurements of downwelling spectral radiance and irradiance, from which are derived optical thicknesses of the atmosphere and its key consituents, and particle size distributions of aerosols based on scattering models for spheres.

The atmospheric optical parameters covered by these protocols (Volume II, Chapter 4 and Volume III, Chapter 5) are aerosol optical thickness (AOT), ozone optical thickness, and aerosol size distributions inferred from downwelling radiance distributions at the sea surface ($z = 0^{+}$). The reader is referred to those chapters and references cited therein for the details of these methods. Here we will introduce only the definitions of optical depth $\tau(z,\lambda)$ and optical thickness $\tau(\lambda)$, and the separation of these into molecular (Rayleigh), ozone and aerosol components.

Optical depth is defined for a vertical path, from $z = 0$ to Z, through a medium as

$$\tau(Z,\lambda)\equiv\int_0^Z c(z,\lambda)dz\ . \tag{2.56}$$

$\tau(z,\lambda)$ is obviously an IOP of the medium, and it increases monotonically with increasing z. ***Optical thickness*** is simply the optical depth over the entire height of the medium, *i.e.* for the atmosphere

$$\tau(\lambda)=\int_0^{Z_{\mathrm{TOA}}} c(z,\lambda)dz \tag{2.57}$$

where Z_{TOA} is the geometric height of the top of the atmosphere. Recalling the additive property of IOP, the total optical thickness of the atmosphere may be expressed as the sum of its components

$$\tau(\lambda)=\tau_{\mathrm{R}}(\lambda)+\tau_{\mathrm{O_3}}(\lambda)+\tau_{\mathrm{a}}(\lambda), \tag{2.58}$$

where τ_R is the Rayleigh optical thickness representing molecular absorption and scattering by the non-variable gases making up the earth's atmosphere, τ_{O_3} is the optical thickness due to absorption by ozone (the only variable gas of importance in ocean color remote sensing), and τ_a is AOT due to scattering and absorption by aerosols.

In methods described in Volume II, Chapter 4 and Volume III, Chapter 5, sun photometers are used to measure direct solar irradiance $E_N\left(0^+,\lambda,\theta_o,\phi_o\right)$, on a plane normal to the solar beam, transmitted downward through the atmosphere. Assuming single scattering, and a plane-parallel medium, this measurement is governed by the solution to equation (2.31) integrated over the entire atmosphere to obtain

$$E_N\left(0^+,\lambda,\theta_o,\phi_o\right) = \overline{F}_o\left(\lambda\right)\left(\frac{d_o}{d}\right)^2 e^{-\frac{1}{\cos\theta_o}\int_0^{z_{TOA}} c(z,\lambda)dz}, \ \mu W\ cm^{-2}nm^{-1}, \tag{2.59}$$

the Beer-Lambert-Bouguer Law, where d_o and d are the mean and actual earth-sun distances, respectively [see equation (4.2) in Volume II, Chapter 4]. In sun photometer measurements, it is necessary to adjust the slant path range to account for curvature of the earth's atmosphere, refraction, and vertical variations in the composition of the atmosphere. The quantity representing this increased path length is called ***air mass*** $M\left(\theta_o\right)$ [see Section 4.1 in Volume II, Chapter 4 and equation (5.3) in Volume III, Chapter 5]. Substituting the adjusted pathlength (air mass) and equations (2.57) and (2.58) in (2.59) leads to the operational equation used to determine AOT as

$$E_N\left(0^+,\lambda,\theta_o,\phi_o\right) = \overline{F}_o\left(\lambda\right)\left(\frac{d_o}{d}\right)^2 e^{-M(\theta_o)\left[\tau_R(\lambda)+\tau_{O_3}(\lambda)+\tau_a(\lambda)\right]}, \ \mu W\ cm^{-2}nm^{-1}. \tag{2.60}$$

The reader is referred to Volume II, Chapter 4 and Volume III, Chapter 5 for details, but basically, $\tau_R\left(\lambda\right)$ is modeled and adjusted for surface atmospheric pressure and elevation, total column ozone concentration is determined independently (either from surface photometer or satellite measurements at selected ultraviolet wavelengths defining the depth of strong ozone absorption bands) and used to compute $\tau_{O_3}\left(\lambda\right)$ at visible and near-infrared wavelengths of interest here, and $E_N\left(0^+,\lambda,\theta_o,\phi_o\right)$ is measured. Equation (2.60) may then be solved for $\tau_a\left(\lambda\right)$ as the only remaining unknown.

2.9 EXTRATERRESTRIAL SOLAR FLUX SPECTRUM

SeaWiFS, MODIS and CZCS algorithms, are all predicated on using a single determination of the spectrum of extraterrestrial solar irradiance for the average distance between the earth and sun, $\overline{F}_o\left(\lambda\right)$. Within the SeaWiFS and MODIS ocean color remote sensing and ocean optics communities, for instance, the presently accepted extraterrestrial solar flux spectrum is that of Neckel and Labs (1984). There is less unanimity in the atmospheric community, and in some segments of the international remote sensing community, in the choice of a "standard" solar spectrum (*e.g.*, MERIS).

It is important that a single, common standard solar flux spectrum be used in every aspect of research and validation in ocean color remote sensing. The extraterrestrial solar flux enters into normalization of water leaving radiance, calibration and interpretation of atmospheric radiation measurements, and atmospheric correction algorithms for all satellite ocean color radiometers. For example, if normalized water leaving radiance were computed from *in situ* measurements using a "better" estimate of the solar flux, in lieu of Neckel and Labs (1984), a comparison with a satellite determination of normalized water-leaving radiance would be biased by the difference between the two solar spectra. There is some evidence (Biggar 1998; Schmid *et al*. 1998) that the recent measurements of Thuillier *et al*. (1998a, 1998b) are more consistent with NIST traceable lamp-based irradiance and radiance sources. On the basis of such findings, it seems clear that NASA and the international ocean color community should reconsider the choice of a standard for extraterrestrial solar flux. Assuming that a change would improve the uncertainty budget of, *e.g*. atmospheric correction validations, the expected benefits are obvious. On the other hand, adopting a different solar spectrum would require significant changes in the software used for operational processing and validation analyses within SeaWiFS, MODIS and other ocean color satellite project offices. Any such transition must be planned and implemented comprehensively in a forum that embraces the entire international community.

The choice of any of the published $\overline{F}_o(\lambda)$ scales cited above will have no discernable effect on the internal uncertainty budget of the vicarious calibration for any individual satellite ocean color sensor (M. Wang, Pers. Comm.). Exact normalized water leaving radiances $L_{WN}^{ex}(\lambda)$ determined from a satellite sensor depend only on atmospheric transmittance, solar zenith angle and earth sun distance, as $\overline{F}_o(\lambda)$ cancels in the determination of $L_{WN}(\lambda)$ [equation (13.18)]. Therefore, $L_{WN}^{ex}(\lambda)$ determinations are directly comparable between two sensors without consideration of the choices of $\overline{F}_o(\lambda)$ scales. The consequences of arbitrary $\overline{F}_o(\lambda)$ scale selections between sensors are:

1. The ratios of sensor-specific $\overline{F}_o(\lambda)$ scales values must be used to directly compare aperture radiances measured above the atmosphere $\left[L_{TOA}(\lambda)\right]$ by two sensors using different $\overline{F}_o(\lambda)$ scales for vicarious calibration;

2. When measured surface irradiance at sea level is used to determine $L_{WN}(\lambda) = L_W(\lambda,\theta,\phi)\dfrac{\overline{F}_o(\lambda)}{E_S(\lambda)}$ [equation (4.8) in Volume III, Chapter 4] from *in situ* field radiometric data, $L_{WN}(\lambda)$ and $L_{WN}^{ex}(\lambda)$ must be computed using the particular $\overline{F}_o(\lambda)$ scale of each sensor to which that data is to be compared. On the other hand, if the same method used to determine $L_{WN}(\lambda)$ for a satellite sensor is used with *in situ* data [equation (4.18) in Volume III, Chapter 4], *e.g.* as with the MOBY $L_{WN}(\lambda)$ time-series (Volume VI, Chapter 2), differences in $\overline{F}_o(\lambda)$ scales need not be considered. The uncertainty budget of the second (4.18) approach is dominated by uncertainties in the modeled atmospheric transmittance, and neglect of cloud effects in the model. Atmospheric transmittance and cloud effects are included implicitly in measured, actual $E_S(\lambda)$, and the uncertainty budget of the first (4.8) approach combines the uncertainties of $E_S(\lambda)$ measurements and the selected $\overline{F}_o(\lambda)$ scale. Present knowledge of the relative uncertainties of $L_{WN}^{ex}(\lambda)$ determined using these two approaches is insufficient to justify a clear-cut choice of a preferred method.

The three alternatives are:

1. Ignore the matter, leave the choice of $\overline{F}_o(\lambda)$ scale to each ocean color sensor team, and do not use measured surface irradiances to determine $L_{WN}^{ex}(\lambda)$ from *in situ* measurements used for validation or vicarious calibration;

2. Publish the particular $\overline{F}_o(\lambda)$ adopted by each satellite ocean color sensor project, thus allowing the use of measured $E_S(\lambda)$ in the determination of $L_{WN}^{ex}(\lambda)$ from *in situ* field data; or

3. Adopt a common international standard scale of $\overline{F}_o(\lambda)$ for use by the entire international ocean color community with all satellite ocean color sensors and associated *in situ* validation data.

Option 1 is the obviously simplest to implement, and it is not mutually exclusive with Option 2. Neither is Option 2 difficult to implement, since it requires only that each satellite ocean color sensor project publish the $\overline{F}_o(\lambda)$ scale that it uses. Option 3 would be more transparent to the user, in that one need not pay attention to which $\overline{F}_o(\lambda)$ scale to use with a particular satellite sensor for any purpose, but it may be more costly and difficult to implement. An informal working group is currently considering these issues and options under the auspices of the International Ocean Color Coordinating Group (IOCCG).

Pending future recommendations by the IOCCG, the present Ocean Optics Protocols assume that any analysis, or application, involving extraterrestrial solar irradiance $\overline{F}_o(\lambda)$ uses the scale of Neckel and Labs (1984).

Appropriate adjustments must be made when the protocols are applied to data from satellite ocean color sensors, including MERIS and GLI, which have been processed using the $\overline{F}_o(\lambda)$ scale of Thuillier *et al*. (1998a, 1998b).

REFERENCES

Austin, R.W., 1974: The remote sensing of spectral radiance from below the ocean surface. In: Optical Aspects of Oceanography, N.G. Jerlov and E.S. Nielson, Eds., pp 317-344.

Austin, R.W. and G. Halikas, 1976: The index of refraction of seawater. *SIO Ref. 76-1*, Vis. Lab., Scripps Inst. of Oceanography, La Jolla, California, 64pp.

Biggar, S.F. 1998: Calibration of a visible and near-infrared portable transfer radiometer. *Metrologia*, **35**: 701-706.

Cox, C. and W. Munk, 1954. Measurement of the roughness of the sea surface from photographs of the sun's glitter. *J. of the Opt Soc. of Am.* **44**(11). 838-850.

Fargion, G.S. and J.L. Mueller, 2000: *Ocean Optics Protocols for Satellite Ocean Color Sensor Validation, Revision 2*, NASA TM 2001-209955, NASA Goddard Space Flight Center, Greenbelt, Maryland, 184

Gordon, H.R., D.K. Clark, J.W. Brown, O.B. Brown, R.H. Evans, and W.W. Broenkow, 1983. Phytoplankton pigment concentrations in the middle Atlantic bight: comparison of ship determinations and CZCS estimates. *Appl. Opt.* **22**(1): 20-36.

Jerlov, N.G., 1976: *Marine Optics*, Elsevier, New York, 231pp.

Liou, K-N, 1980: *An Introduction to Atmospheric Radiation*, Academic Press, New York, 392pp.

Mobley, C.D., 1994: *Light and Water; Radiative Transfer in Natural Waters*. Academic Press, San Diego, California. 592pp.

Mobley, C.D., 1999: Estimation of the remote-sensing reflectance from above-surface measurements. *Appl. Opt*. **38**: 7442-7455.

Morel, A., 1974: Optical properties of pure water and pure sea water. In: *Optical Aspects of Oceanography*, N.G. Jerlov and E.S. Nielson, Eds., pp1-23.

Morel, A., and B. Gentili, 1991: Diffuse reflectance of oceanic waters. I. Its dependence on sun angle as influenced by the molecular scattering contribution. *Appl. Opt*., **30**, 4,427-4,438.

Morel, A., and B. Gentili, 1993: Diffuse reflectance of oceanic waters. II. Bidirectional aspects. *Appl. Opt*. **32**: 6,864-6,879.

Morel, A., and B. Gentili, 1996: Diffuse reflectance of oceanic waters. III. Implication of bidirectionality for the remote-sensing problem. *Appl. Opt*. **35**: 4850-4862.

Morel, A. and R.C. Smith, 1982. Terminology and Units in Optical oceanography. *Marine Geodesy*, **5**(4). 335-350.

Mueller, J.L. and R.W. Austin, 1992: Ocean Optics Protocols for SeaWiFS Validation. *NASA Tech. Memo. 104566, Vol. 5,* S.B. Hooker and E.R. Firestone, Eds., NASA Goddard Space flight center, Greenbelt, Maryland, 45 pp.

Mueller, J.L. and R.W. Austin, 1995: Ocean Optics Protocols for SeaWiFS Validation, Revision 1. *NASA Tech. Memo. 104566, Vol. **25,*** S.B. Hooker and E.R. Firestone, Eds., NASA Goddard Space flight center, Greenbelt, Maryland, 66 pp.

Mueller, J.L. and G.S. Fargion, 2002: *Ocean Optics Protocols for Satellite Ocean Color Sensor Validation, Revision 3*, NASA TM 2002-210004, NASA Goddard Space Flight Center, Greenbelt, Maryland, 308pp

Neckel, H., and D. Labs, 1984: The solar radiation between 3,300 and 12,500 AA. *Solar Phys*., **90**: 205--258.

Preisendorfer, R.W. 1960: *Recommendation on the standardization of concepts, terminology and notation of hydrologic optics*. Scripps Inst. Of Oceanogr., SIO Report, 96pp.

Preisendorfer, R.W. 1964: A model for radiant distribution in natural hydrosols. In: *Physical Aspects of Light in the Sea,* J.C. Tyler [Ed.]. Univ. Hawaii Press, Honolulu, Hawaii, pp. 51-60.

Preisendorfer, R.W., 1976: Hydrologic Optics, in 6 volumes: Vol. 1: Introduction, 218pp (NTIS PB-259 793/8ST); Vol. 2: Foundations, 400 pp (NTIS PB-259 794/6ST); Vol. 3: Solutions, 246 pp (NTIS PB-259 795/3ST); Vol. 4: Imbeddings, 207 pp (NTIS PB-259 796/1ST); Vol. 5: Properties, 296 pp (NTIS PB-259 797/9ST); Vol. 6: Surfaces, 390 pp (NTIS PB-268 704/4ST), Pacific Mar. Environ. Lab/NOAA Seattle, WA. (Available from Natl. Tech. Inform. Serv., Springfield, VA 22161, using the above NTIS numbers.)

Schmid, B., P.R. Spyak, S.F. Biggar, C. Wehrli, J. Seider, T. Ingold, C. Matzler and N. Kampfer. 1998: Evaluation of the applicability of solar and lamp radiometric calibrations of a precision Sun photometer operating between 300 and 1025 nm. *Appl. Opt*. **37**: 3923-3941.

Thuillier, G., M. Herse, P.S. Simon, D. Labs, H. Mandel, D. Gillotay and T. Foujols. 1998a: The visible solar spectral irradiance from 350 to 850 nm as measured by the SOLSPEC spectrometer during the Atlas I mission. *Solar Phys.* **177**: 41-61.

Thuillier, G., M Herse, P.C. Simon, D. Labs, H. Mandel and D. Gillotay, 1998b: Observation of the solar spectral irradiance from 200 nm to 870 nm during the ATLAS 1 and ATLAS 2 missions by the SOLSPEC spectrometer. *Metrologia*, **35**: 689-695.

Chapter 3

Data Requirements for Ocean Color Algorithms and Validation

James L. Mueller[1], Giulietta S. Fargion[2] and Charles R. McClain[3]

[1]*Center for Hydro-Optics and Remote Sensing, San Diego State University, California*
[2]*Science Applications International Corporation, Beltsville, Maryland*
[3]*NASA, Goddard Space Flight Center, Greenbelt, Maryland*

3.1 INTRODUCTION

The principal *in situ* variables to be measured, or derived from measurements, for satellite ocean color sensor validation, and algorithm development and validation, are listed in Table 3.1. The variables are grouped, in Table 3.1, into four related groups: Radiometric Quantities (both oceanic and atmospheric), Inherent Optical Properties (IOP) of sea water, Biogeochemical and Bio-Optical Properties of sea water, and Ancillary Data and Metadata required to support the use, analysis, interpretation, and quality assessment of the other data. Those *in situ* variables that are measured are classified into three categories of descending priority.

The first category of measurements, flagged "Required" in Table 3.1, is the minimum subset required for validating a satellite sensor's radiometric performance, exact normalized water-leaving radiances (Volume III, Chapter 4), and fundamental derived products, including chlorophyll a concentration, aerosol optical thickness, and $K(490)$, and for associated algorithm development and validation.

The second category, flagged "Highly Desired" in Table 3.1, are measurements that supplement the minimum subset and are needed for investigations focused on atmospheric correction algorithms and aerosols, relationships between IOP and remote sensing reflectance, and/or Case 2 algorithms.

The third category, flagged "Specialized Measurement" in Table 3.1, are measurements which either address aspects of ocean bio-optics that are secondary to satellite remote sensing, or require highly specialized equipment that is not readily available to the community at large.

A fourth category, flagged as "Derived", comprises key quantities that are either calculated from the *in situ* measurements, or are derived from models. The above set of variables is also listed in Table 3.2, to identify the satellite ocean color sensor application for which each measurement is needed. Table 3.2 also provides an index of the protocol volumes and chapters addressing each *in situ* measurement.

3.2 RADIOMETRIC QUANTITIES

Surface incident spectral irradiance in air, $E_S(\lambda) \equiv E_d(0^+,\lambda)$, downwelled spectral irradiance, $E_d(z,\lambda)$, and upwelled spectral radiance, $L_u(z,\lambda)$, are the fundamental measurable quantities needed to derive normalized water-leaving radiances (or equivalently remote sensing reflectance) in most circumstances. Other radiometric properties listed in Table 3.1, including sky radiance and normal solar irradiance, are also important *in situ* measurements in the SIMBIOS ocean color validation program. Also listed are critical radiometric quantities that are calculated, or derived, from *in situ* measurements. In some cases, listed radiometric quantities may be derived, wholly or in part, from other non-radiometric measurements listed in the table. For example, remote sensing reflectance may either be calculated directly as the ratio of water-leaving radiance $L_W(\lambda)$ to incident irradiance, $L_W(\lambda):E_S(\lambda)$, or it may be modeled as a function of the IOP ratio of the backscattering to absorption coefficients, $b_b(\lambda):a(\lambda)$, and the Bidirectional Reflectance Distribution Function (BRDF) (Volume III, Chapter 4).

Downwelled spectral irradiance, $E_d(z,\lambda)$, is required to compute the diffuse attenuation coefficient, $K_d(z,\lambda)$, which in turn, is needed for diffuse attenuation coefficient algorithm development (Austin and Petzold 1981; Mueller and Trees 1997; Mueller 2000), and for optically weighting the pigment concentrations to be estimated from remotely sensed ocean color (Gordon and Clark 1980). As with $L_u(0^-,\lambda)$, $E_d(z,\lambda)$, must be determined by extrapolation from a profile of $E_d(z,\lambda)$, over the upper few diffuse attenuation lengths and reconciled with the direct surface measurement above the water of $E_S(\lambda)$ plus downward reflection of $E_u(0^-,\lambda)$.

Upwelled spectral radiance, $L_u(0^-,\lambda)$ is the in-water variable which, when propagated upward through the sea surface, leads to the measured value of $L_W(\lambda)$. $L_W(\lambda)$ is, in turn, adjusted using $E_S(\lambda)$ to derive the normalized water-leaving radiance, $L_{WN}(\lambda)$, for a no-atmosphere, zenith sun at the mean earth-sun distance. Unfortunately, it is not practical to measure $L_u(0^-,\lambda)$ precisely at an infinitesimal depth below the surface. Therefore, the profile of $L_u(z,\lambda)$, must be measured over the upper few optical depths with sufficient accuracy to determine $K_L(z,\lambda)$ for $L_u(z,\lambda)$, and to propagate $L_u(z,\lambda)$ to the surface. At near-infrared (NIR) wavelengths, the first optical attenuation length is confined to the upper few tens of centimeters. Determination of $L_u(0^-,\lambda)$, in this situation is more challenging and will require special instruments and experiment designs to accommodate the effects of instrument self-shading, wave focusing, small-scale variability, possible fluorescence, Raman scattering, and extremely small working volumes. Similar complications arise at all wavelengths in case 2 waters. For algorithm development and validation in these difficult cases, measurements of inherent optical properties (IOP), including coefficients of absorption $a(z,\lambda)$, beam attenuation $c(z,\lambda)$ and backscattering $b_b(z,\lambda)$, and spectral fluorescence, may be usefully combined with $E_d(z,\lambda)$, and $L_u(z,\lambda)$ measured with specially designed radiometers, and $L_{sfc}(\lambda,\theta,\phi,\theta_o,\phi_o)$ and $L_{sky}(\lambda,\theta,\phi,\theta_o,\phi_o)$ measured above-water.

Upwelled spectral irradiance, $E_u(z,\lambda)$, is a useful measurement, in addition to $E_d(z,\lambda)$ and $L_u(z,\lambda)$, because there exist both empirical and theoretical relationships between IOP, phytoplankton pigments, SPM, and irradiance reflectance. $L_u(0^-,\lambda)$ and $E_u(0^-,\lambda)$ are related by the factor $Q_n(\lambda)$, which has been shown to vary with solar zenith angle (Volume III, Chapter 4; Morel and Gentili 1993, 1996; Morel, Voss and Gentili 1995). Combined measurements of $L_u(0^-,\lambda)$ and $E_u(0^-,\lambda)$ will be extremely useful in determining $Q_n(\lambda)$, which will in turn, allow traceability of the measurements by the SIMBIOS ensemble of satellite ocean color sensors to previously derived irradiance reflectance relationships and algorithms.

Radiance distribution measurements $L_u(z,\lambda,\theta',\phi')$ just beneath the sea surface will be required for quantifying the angular distribution of water-leaving radiance at stations used for system calibration initialization and long-term system characterization. These measurements will also necessary to determine the BRDF of the water and verify the models used to normalize water-leaving radiance for variations in viewing and solar zenith angles (Volume III, Chapter 4 and references cited therein).

Water Surface Radiance (in air), $L_{sfc}(\lambda,\theta,\phi,\theta_o,\phi_o)$, measured from the deck of a ship (or a low-flying aircraft) is a potentially useful substitute for $L_W(\lambda)$ determined from in-water $L_u(0^-,\lambda)$. The measured surface radiance is the sum of water-leaving radiance and sky radiance reflected from the wave-roughened sea surface. The principal, and significant, source of uncertainty in this approach is associated with removal of reflected sky radiance from the total signal (Volume III, Chapter 3).

Surface incident spectral irradiance, $E_S(\lambda)$, is usually measured on a ship well above the water. In some previous versions of these protocols (Mueller and Austin 1992, 1995), it was suggested that $E_S(\lambda)$ might alternatively be determined from measurements of $E_d(0^-,\lambda)$ made some distance from the ship using a radiometer

floated just beneath the surface. The community has gained experience with this approach and found that wave-induced fluctuations in near-surface irradiance produce an uncertainty in $E_d(0^-,\lambda)$ approaching 10 % in even ideal cases (Siegel *et al.* 1995). $E_S(\lambda)$ varies due to fluctuations in cloud cover and aerosols, and with time of day, *i.e.*, solar zenith angle. Profiles of $E_d(z,\lambda)$, and $L_u(z,\lambda)$, must be normalized to account for these sources of variability during a cast.

Normal Solar Irradiance spectra $E_N(\lambda,\theta_o,\phi_o)$ should be measured using a sun photometer to determine atmospheric transmittance and aerosol optical depths at each station. These data are particularly needed to verify the atmospheric corrections in direct match-up comparisons between satellite ocean color sensor $L_{WN}^{ex}(\lambda)$ estimates and those determined from in-water measurements of $L_u(z,\lambda)$.

Sky radiance, $L_{sky}(\lambda,\theta,\phi,\theta_o,\phi_o)$, is required to enable estimation of the aerosol phase function through inversion of the radiative transfer equation. It is also useful for estimating the mean cosine of the transmitted light field in the water. The sky radiance should be measured directly; for the latter application, however, it need only be estimated by occulting the sun's image on a deck cell measuring the incident spectral radiance from the sun and sky. The mean cosine at the surface can be used with profile measurements of $E_d(z,\lambda)$, $E_u(z,\lambda)$, and $c(\lambda)$ to estimate $b_b(\lambda)$ (Gordon 1991). An ability to exploit this and similar relationships will greatly enhance both development and verification of bio-optical algorithms, especially in case 2 waters. The spectral sky radiance distribution over zenith and azimuth angles is required to determine the aerosol scattering phase functions at radiometric comparison stations during system initialization cruises. It is also measured routinely at a network of fixed island and coastal sites distributed around the world. Finally, $L_{sky}(\lambda,\theta,\phi,\theta_o,\phi_o)$ is measured and multiplied by the reflectance of the sea surface to derive $L_W(\lambda,\theta,\phi)$ from $L_{sfc}(\lambda,\theta,\phi,\theta_o,\phi_o)$ measurements.

Diffuse Sky Irradiance, $E_{sky}(\lambda)$, may be measured using a fast-rotating, shipboard version of a Shadowband Radiometer, or by manually obscuring the direct solar irradiance, $E_{sun}(\lambda)$, component of $E_S(\lambda)$. This measurement is extremely useful for determining the ratio $E_{sun}(\lambda):E_{sky}(\lambda)$, which is a critical factor in self-shading corrections to $L_u(z,\lambda)$ and $E_u(z,\lambda)$ measurements (Gordon and Ding 1992).

3.3 INHERENT OPTICAL PROPERTIES

Inherent Optical Properties (IOP) must be measured for development and validation of the ocean color semi-analytic case 2 chlorophyll *a* algorithm. This algorithm is based on an explicit theoretical function of the ratio of backscattering to absorption, $b_b(\lambda):a(\lambda)$. This ratio is also an important factor in the BRDF models underlying the exact normalization of water-leaving radiance for solar and viewing azimuth and zenith angles (Volume III, Chapter 4). Due to recent advances in instrumentation, it is now practical to routinely measure *in situ* profiles of *absorption* $a(z,\lambda)$, *beam attenuation* $c(z,\lambda)$ and *backscattering* $b_b(z,\lambda)$ coefficients. The scattering coefficient may therefore also be obtained as $b(z,\lambda)=c(z,\lambda)-a(z,\lambda)$. The IOP also provide critical factors in the Gordon and Ding (1992) model used to correct upwelled radiance and irradiance measurements for instrument self shading. Future algorithm development and validation experiments involving these algorithms must, therefore, include absorption, beam attenuation, and backscattering measurements. It is anticipated that new instruments, now under development and testing, will allow *in situ* measurements of the volume scattering function $\beta(z,\lambda,\Psi)$ (Volume I, Chapter 2 and Volume IV, Chapter 5). Measurements of $\beta(z,\lambda,\Psi)$ will be very useful in advancing remote sensing reflectance models and algorithms involving the BRDF (Volume III, Chapter 4).

The *particle absorption coefficient*, $a_p(z,\lambda)$, which is comprised of absorption by living, dead, and inorganic particles, is a useful variable for modeling the portion of solar energy that is absorbed by phytoplankton and bacteria. A laboratory spectrophotometer may be used to measure $a_p(z,\lambda)$ of particles filtered from seawater

samples collected at depth z, or it may be computed as the difference between *in situ* measurements with a pair of filtered (CDOM absorption) and unfiltered (total absorption) instruments.

The *colored dissolved material (CDOM) absorption coefficient,* $a_g(z,\lambda)$, is an important contributor to total absorption in many coastal waters. Because CDOM, variously referred to as *gelbstoffe, gilvin,* or *yellow-matter*, absorbs very strongly in the blue, its undetected presence can create large regional uncertainties in chlorophyll a retrievals from ocean color image data. The CDOM absorption coefficient $a_g(z,\lambda)$ may either be measured *in situ* by installing a 0.2 μm filter in the water intake port of an absorption and beam attenuation meter, or in the laboratory using a spectrophotometer to measure absorption by filtered seawater, typically over a 10 cm path.

The non-pigmented particle absorption coefficient, $a_d(z,\lambda)$, accounting for absorption of light by detritus (or tripton), represents a major loss of light which would otherwise be available to the phytoplankton component of the marine hydrosol. In many cases, absorption by detritus is a significant term in the marine radiative transfer processes, and its determination is useful for phytoplankton production models and for modeling the light field. The spectral absorption coefficient $a_d(z,\lambda)$ using the $a_p(z,\lambda)$ filters, after they are washed with hot methanol to remove phytoplankton pigments (Volume IV, Chapter 4).

3.4 BIOGEOCHEMICAL AND BIO-OPTICAL QUANTITIES

Phytoplankton pigment composition will be determined using the *HPLC* method to develop and validate ocean color pigment algorithms, and to assess the effects of accessory pigment concentrations on water-leaving spectral radiances (Volume V, Chapter 2). These data may also be used to calibrate continuous profiles of *in situ* fluorescence. *Chlorophyll a and pheopigment concentrations* will also be determined using the *fluorometric method* (Volume V, Chapter 3). The HPLC chlorophyll *a* concentrations are more accurate than fluorometric concentrations, which are often biased systematically throughout a particular geographic region and time of year. On the other hand, fluorometric measurements of chlorophyll a concentration are both far easier and less expensive to perform, allowing a far greater number of pigment validation samples to be acquired on a given cruise than if HPLC sampling were used alone. If a well-distributed subset of pigment filter samples from each validation cruise are reserved for HPLC measurements, it is possible and operationally effective to derive regional and temporal corrections to scale fluorometric and HPLC chlorophyll a concentrations into close agreement.

Phycobilipigments, present in cyanobacteria and cryptophytes, are treated separately from the HPLC fat-soluble pigments. Phycoerythrin and phycocyanin are the two major groups of phycobilipigments found in the marine environment. The concentration of these water-soluble pigments is important due to the contribution of solar stimulated phycoerythrin fluorescence to the underwater light field, and also to characterize the phytoplankton population. At times, species that contain phycobilipigment can account for a large fraction of the primary productivity (especially in oligotrophic waters) and have been difficult to quantify due to their small size. Although neither SeaWiFS nor MODIS contains bands at the absorption or fluorescence peaks of phycobilipigments, future satellite ocean color sensors, including GLI and MERIS will have appropriate bands. The present protocols do not specify methods for measuring phycobilipigments, but qualitative concentrations may be obtained today using a fluorometric approach, and a new capillary electrophoresis method is currently under development (C. Kinkade, personal comm.). A new chapter giving protocols for measuring this important group of phytoplankton pigments may emerge in a future revision to Volume V.

Coccolith concentration, which is the number density of small plates (coccoliths) composed of calcium carbonate ($CaCO_3$), is very important to light scattering. Coccoliths are produced in copious amounts by marine phytoplankton called coccolithophorids. Scattering of light by coccoliths is highly apparent in visible wavelength satellite imagery, because they perturb the usual relationships between water-leaving radiances and pigment concentration, and therefore, adversely impact atmospheric corrections (Balch *et al.* 1991, Voss *et al*. 1998). Additionally, coccolith formation, sinking, and dissolution are significant factors in the ocean carbon flux budget. It is, therefore, necessary to measure coccolith concentration, both as number density and $CaCO_3$ concentration, to aid in 1) the correction of chlorophyll a concentration algorithms, 2) coccolith algorithm development, and 3) atmospheric correction development and validation. This present version (4.0) of the ocean optics protocols does not cover methods for measuring coccolith concentration, except as summarized in Volume V, Chapter 1. Such protocols may be included in a future revision to Volume V.

Total Suspended Matter (SPM) measurements are required to assess the effect of suspended sediment on the derived products. SPM is of primary importance in coastal waters, where simple radiance ratio algorithms for SPM have uncertainties equivalent to, or greater than, those for estimating chlorophyll-like pigment concentration. Organic suspended matter and inorganic suspended matter concentrations are fractions of SPM; this partitioning of SPM is particularly useful in process studies.

Continuous profile measurements of *in situ chlorophyll a fluorescence intensity* are exceptionally useful as guidance in analyzing profiles of $E_{\mathrm{d}}(z,\lambda)$, $L_{\mathrm{u}}(z,\lambda)$, and $E_{\mathrm{u}}(z,\lambda)$ to derive profiles of $K_{\mathrm{d}}(z,\lambda)$, $K_{\mathrm{L}}(z,\lambda)$, and $K_{\mathrm{u}}(z,\lambda)$, respectively. Moreover if these profiles are viewed in real time, they are also useful guides for taking water samples at depths that allow the vertical structure of pigment concentration profiles to be accurately resolved in the top optical depth and to determine subsurface maxima in chlorophyll concentration. Finally, the continuous *in situ* chlorophyll *a* fluorescence profile may be used to interpolate HPLC, or extracted fluorescence, measurements of chlorophyll *a* concentrations from water samples at discrete depths. It is desirable to make these measurements simultaneously with IOP profiles, and also those of irradiance and radiance if it can be done in a way to avoid self-shading of the radiometers.

3.5 ANCILLARY DATA AND METADATA

The geographic location and time at which *in situ* validation data are acquired are essential information that must be included in every data submission under the SIMBIOS program. The obvious metadata items in this context are *latitude, longitude, date and time (UTC)*. Expressing date and time in UTC is also essential, even though it may be helpful to also list local date and time with a validation station's metadata. Too often, field investigators neglect to identify (or possibly even keep track of) the time zone used by a data-logging computer to enter time into data records.

Sea state, expressed as significant wave height in m, must be reported with *in situ* validation measurements. *Whitecap conditions*, expressed as the estimated fractional area covered, are also useful and highly desired. Digital photographs documenting surface wave and whitecap conditions during radiometric measurements are also helpful. This information is essential for identifying measurements made under questionable environmental conditions.

Wind speed and direction are required to generate, through models, estimates of the surface wave slope distribution, which will be used to calculate reflected skylight and sun glint in radiative transfer models (Cox and Munk 1954). Wind speed is an essential parameter for computing exact normalized water-leaving radiance from measured water leaving radiance emerging from the ocean at zenith angles greater than 25^{o} (Volume III, Chapter 4). Surface wave models driven by wind velocity may also be used to provide quantitative estimates of surface wave induced radiometric fluctuations. Qualitatively, wind velocity, and photographs or videotape recordings of sea state, will be useful for assessing station data quality.

Surface barometric pressure measurements are required to validate both atmospheric correction algorithms and the surface pressures derived from operational weather analyses for use in processing satellite ocean color data

Cloud cover (expressed as fractional coverage in octals, or percent) is essential metadata used for assessing data quality and screening questionable cases from algorithm development and validation analyses. A description of sky conditions near the sun and satellite zenith and azimuth angles, including whether the sun is obscured during observations, is also important information. Cloud type information is also useful, as are photographs of sky conditions.

Secchi depth measurements are required for real-time assessment of water transparency during a station and as a quality check during analysis of radiometric profiles.

Water depth, z in m, is important information for screening data from shallow water cases where bottom reflections may be present in water-leaving radiance measurements.

Hydrographic data, *water temperature (T), and salinity (S)*, derived from *conductivity, temperature, and depth (CTD)* profiles, are useful for characterizing the physical water mass regime in which an optical profile is measured. A *T-S* characterization is especially important near ocean fronts and eddies where interleaving water masses of very different biogeochemical composition, and therefore fundamentally different bio-optical properties, can produce complex spatial and temporal patterns of near-surface optical properties. In these circumstances, *T-S* profiles can

provide an indication of whether a station location is suitable for reliable remote sensing validation and algorithm development comparisons. The *T(z)* and *S(z)* measurements are also needed for corrections to pure water absorption in processing IOP measurements.

3.6 PROCESS MODEL RELATED DATA

Other types of *in situ* measurements are also important in the context of ocean color validation, because they are needed either to support, or validate, process models that are derived with the aid of ocean color image data. Primary productivity models are, perhaps, the foremost example of these secondary products of satellite ocean color measurements. The *in situ* measurements needed to support such models, and other scientific investigations and applications that may exploit ocean color data products, are undeniably important and closely related to the quantities listed in Table 3.1. These measurements are not, however, essential to algorithm development and validation of products derived from the ocean color data directly. In the future, the scope of the ocean optics protocols may be expanded to embrace methods for measuring and/or analyzing some of these variables, but at present they are not included. Some of the more important measurements of this class are briefly described in this section, but none of them are discussed in detail.

Aerosol concentration samples using high volume techniques will be useful, in conjunction with aerosol optical depth spectra determined from sun photometer measurements, for chemical, size, and absorption characterization of aerosols, especially in studies of the effects of Saharan and Asian dust clouds on atmospheric corrections.

Particulates, both Particulate Organic Carbon (POC) and Particulate Organic Nitrogen (PON), are required for process studies to help characterize the adaptive state of phytoplankton and to inventory critical biogeochemical elements.

Dissolved Organic Carbon (DOC) has been shown to be a major pool of carbon in the oceans. Quantification of the transformations of this pool is crucial to understanding the marine carbon cycle. The Colored Dissolved Organic Material (CDOM) fraction of the DOC is highly absorbent in the blue range, thus decreasing blue water-leaving radiances, and it must be taken into consideration for pigment concentration algorithms. DOC measurements are needed to develop robust relationships between CDOM and DOC, which are needed to evaluate the usefulness of ocean color observations for estimating DOC concentrations.

CDOM concentrations are required to assess the effect of *Gelbstoff* on blue water-leaving radiances and chlorophyll concentration. This is of primary importance in case 2 waters, but is also relevant to phytoplankton degradation products in case 1 waters.

Humic and fulvic acids comprise the bulk of CDOM and have different specific spectral absorption coefficients. Their concentrations are useful for determining the correction used for phytoplankton pigment concentration algorithms in case 2 waters and for estimating CDOM from ocean color observations.

Particle size spectra are very useful for in-water radiative transfer calculations, particularly if measurements include particles smaller than 1 μm.

Particle fluorescence, measured using laser sources in single-cell flow systems, may be used to calculate particle scattering-to-fluorescence ratios for evaluating the population structure of the plankton (both phyto- and zooplankton).

Phytoplankton species counts are important because species-to-species variability in optical and physiological properties represents a major source of variability in bio-optical algorithms and primary productivity models. This has been recognized, but it is generally ignored in remote sensing algorithms due to the tedious nature of species enumeration, the small sizes of many species, and the large number of species involved. This information, however, at various levels of rigor, is useful in evaluating the population and pigment composition. This is especially important for some groups, such as coccolithophorids.

Primary productivity, using the radioactive isotope ^{14}C estimation method, is not strictly required for validation of water-leaving radiances or system initialization. It is a MODIS product and will be a SeaWiFS product in the future. It will, moreover, be extremely useful for process study applications of ocean color data if these measurements are made at the same time that the water column optical properties are determined. These data will aid in the development of models of primary production using satellite ocean color observations, a goal that is central to all global ocean color mission. Of special importance are determinations of key photo-physiological

parameters derived from production measurements as functions of irradiance. If ^{14}C productivity measurements are made, they should conform to the *JGOFS Core Measurements Protocols* (UNESCO 1994).

REFERENCES

Austin, R.W., and T.J. Petzold, 1981: The determination of diffuse attenuation coefficient of sea water using the Coastal Zone Color Scanner. *Oceanography from Space*, J.F.R. Gower, Ed., Plenum Press, 239-256.

Balch, W.M., P.M. Holligan, S.G. Ackleson, and K.J. Voss, 1991: Biological and optical properties of mesoscale coccolithophore blooms in the Gulf of Maine. *Limnol. Oceanogr.*, **36**, 629-643.

Cox, C., and W. Munk, 1954: Measurements of the roughness of the sea surface from photographs of the sun's glitter. *J. Opt. Soc. Am.,* 44, 838--850.

Gordon, H.R., 1991: Absorption and scattering estimates from irradiance measurements: Monte Carlo simulations. *Limnol. Oceanogr*., **36**: 769--777.

Gordon, H.R., and D.K. Clark, 1980: Remote sensing optical properties of a stratified ocean: an improved interpretation. *Appl. Optics*,**19**: 3,428--3,430.

Gordon, H.R., and K. Ding, 1992: Self shading of in-water optical instruments. *Limnol. Oceanogr*., **37**, 491-500.

Morel, A., and B. Gentili, 1993: Diffuse reflectance of oceanic waters. II. Bidirectional aspects. *Appl. Opt*., **32**: 6,864--6,879.

Morel, A., and B. Gentili, 1996: Diffuse reflectance of oceanic waters. III. Implication of bidirectionality for the remote-sensing problem. *Appl. Optics*, **35**: 4850-4862.

Morel, A., K.J. Voss, and B. Gentili, 1995: Bidirectional reflectance of oceanic waters: a comparison of modeled and measured upward radiance fields. *J. Geophys. Res.***100**: 13,143-13,151.

Mueller, J.L., and R.W. Austin, 1992: Ocean Optics Protocols for SeaWiFS Validation. *NASA Tech. Memo. 104566, Vol. 5,* S.B. Hooker and E.R. Firestone, Eds., NASA Goddard Space Flight Center, Greenbelt, Maryland, 43 pp.

Mueller, J.L., and R.W. Austin, 1995: Ocean Optics Protocols for SeaWiFS Validation, Revision 1. *NASA Tech. Memo. 104566, Vol. 25,* S.B. Hooker, E.R. Firestone and J.G. Acker, Eds., NASA Goddard Space Flight Center, Greenbelt, Maryland, 67 pp.

Mueller, J.L. and C.C. Trees, 1997: Revised SeaWiFS prelaunch algorithm for the diffuse attenuations coefficient K(490). In: Yeh, et al. Case Studies for SeaWiFS Calibration and Validation, Part 4. *NASA Tech. Memo. 104566, Vol. 41,* S.B. Hooker, E.R. Firestone and J.G. Acker, Eds., NASA Goddard Space Flight Center, Greenbelt, Maryland, 18-21.

UNESCO, 1994: Protocols for the Joint Global Ocean Flux Study (JGOFS) Core Measurements. *JGOFS Manuals and Guides, 29*, Scientific Committee on Oceanic Research, 40 p.

Siegel, D.A., M.C. O'Brien, J.C. Sorensen, D.A. Konnoff, E.A. Brody, J.L. Mueller, C.O. Davis, W.J. Rhea, and S.B. Hooker, 1995. Results of the SeaWiFS Data Analysis Round-Robin, July 1994 (DARR-94). *NASA Tech. Memo. 104566, Vol. 26*, S.B. Hooker and E.R. Firestone, Eds., NASA Goddard Space Flight Center, Greenbelt, MD. 58pp.

Voss, K.J., W.M. Balch and K.A. Kilpatrick, 1998: Scattering and attenuation properties of Emiliania huxleyi cells and their detached coccoliths, *Limnol. Oceangr.,* **43**(5): 870-876.

Table 3.1: Principal *in situ* observations for satellite ocean color system validation, and algorithm development and validation. The right-hand column identifies and classifies measurements as: (a) required for minimal validation match-ups; (b) highly desired and important for general algorithm development and validation; (c) specialized measurements of important, but restricted, applicability to algorithm development and validation (for the present); and (d) calculated or derived quantities.

	Required	Highly Desired	Specialized Measurement	Derived
Radiometric Quantities				
Downwelled Irradiance $E_d(z,\lambda)$	✓			
Upwelled Radiance $L_u(z,\lambda) = L(z, \lambda,0,0)$	✓			
Upwelled Irradiance $E_u(z,\lambda)$			✓	
Radiance Distribution in water $L(z, \lambda,\theta',\phi')$			✓	
Water Surface Radiance in air $L_{sfc}(\lambda,\theta,\phi)$		✓		
Incident Irradiance in air $E_s(\lambda) = E_d(0^+,\lambda)$	✓			
Normal Solar Irradiance $E_N(\lambda, \theta_o,\phi_o)$	✓			
Sky Radiance $L_{sky}(\lambda,\theta,\phi)$		✓		
Diffuse Sky Irradiance $E_{sky}(\lambda)$		✓		
Direct Sun Irradiance $E_{sun}(\lambda) = E_s(\lambda) – E_{sky}(\lambda)$				✓
Water-Leaving Radiance $L_w(\lambda,\theta,\phi,\theta_o,\phi_o)$				✓
Remote Sensing Reflectance $R_{RS}(\lambda,\theta,\phi,\theta_o,\phi_o)$				✓
Attenuation Coefficient $K(z,\lambda)$ for $E_d(z,\lambda)$ and $L_u(z,\lambda)$				✓
Ocean Bidirectional Reflectance Distribution Function BRDF				✓
Aerosol Optical Depth $\tau_a(\lambda)$	✓			
Aerosol Phase Function $P_a(\lambda,\Psi)$				✓
Absorbing Aerosol Height Profiles (LIDAR Profilometer)			✓	
Inherent Optical Properties				
Beam Attenuation Coefficient $c(z,\lambda)$		✓		
Absorption Coefficient $a(z,\lambda)$		✓		
Backscattering Coefficient $b_b(z,\lambda)$		✓		
Scattering Coefficient $b(z,\lambda) = c(z,\lambda) - a(z,\lambda)$				✓
Volume Scattering Function $\beta(z, \lambda,\Psi)$			✓	
Particle Absorption Coefficient $a_p(z,\lambda)$		✓		✓
Dissolved Material (CDOM) Absorption Coefficient $a_g(z,\lambda)$		✓		
Non-Pigmented Particle Absorption Coefficient $a_d(z,\lambda)$		✓		
Phytoplankton Absorption Coefficient $a_\phi(z,\lambda)$		✓		
Biogeochemical and Bio-Optical Quantities				
Phytoplankton Pigment Composition (HPLC method)	✓			
Chlorophyll *a* and Phaeopigments Conc. (Fluorometric method)	✓			
Phycobiliprotein Concentrations			✓	
Coccolith Concentrations			✓	
Total Suspended Particulate Material (SPM)			✓	
Particle Size Distribution			✓	
Particulate Organic Carbon (POC)			✓	
Particulate Organic Nitrogen			✓	
Fluorescence Intensity, *in situ* profile $F(z)$		✓		

Table 3.1 Continued.

	Required	Highly Desired	Specialized Measurement	Derived
Ancillary Data and Metadata				
Latitude and Longitude	✓			
Date and Time (UTC)	✓			
Wave Height	✓			
Whitecap Conditions (fractional amount of surface)		✓		
Wind Speed, W, and Direction	✓			
Surface Barometric Pressure	✓			
Cloud Cover (amount, and sun obscuration information)	✓			
Cloud Type		✓		
Secchi Depth	✓			
Water Depth	✓			
Conductivity and Temperature over Depth (CTD) $T(z)$, $S(z)$		✓		

Table 3.2: Principal *in situ* observations for satellite ocean color system validation, and algorithm development and validation. The right-hand column identifies the protocol chapters and suggested applications. The application keys are: System Validation (1); Radiometric System Performance Validation and Vicarious Calibration (2); Atmospheric Correction Validation (3); Atmospheric Product Validation (4); Bio-Optical Product Validation (5); Algorithm Development and Validation (6); Atmospheric Property and Correction Algorithms (7); Bio-Optical Algorithms (8); IOP Algorithms and Semi-Analytic IOP-Based Algorithms (9); Normalized $L_{WN}(\lambda)$ and $R_{RS}(\lambda)$ Algorithms (10); Metadata (all applications) (11) ; Quality Control (12); and All Above Applications (13).

	Protocol Chapters (Volume)	Applications Keys
Radiometric Quantities		
Downwelled Irradiance $E_d(z,\lambda)$	2 (III)	1,5,6,8-10
Upwelled Radiance $L_u(z,\lambda) = L(z, \lambda,0,0)$	2, 3 (III), 2, 3 (VI)	1-3,5,6,8-10
Upwelled Irradiance $E_u(z,\lambda)$	2 (III)	6,9,10
Radiance Distribution in water $L(z, \lambda,\theta,\phi)$	TBD	1,2,6,9,10
Water Surface Radiance in air $L_{sfc}(\lambda,\theta,\phi)$	3 (III)	1-3,5,6,8-10
Incident Irradiance in air $E_s(\lambda) = E_d(0^+,\lambda)$	4 (II), 2-5 (III), 2,3 (VI)	1,6,8,9,10,13
Normal Solar Irradiance $E_N(\lambda,\theta_o,\phi_o)$	4 (II), 5 (III)	1-4,6,7,10,12
Sky Radiance $L_{sky}(\lambda,\theta,\phi)$	4 (II), 5 (III)	1-4,6,7,10
Diffuse Sky Irradiance $E_{sky}(\lambda)$	4 (II),2, 5 (III)	1,6,13
Direct Sun Irradiance $E_{sun}(\lambda) = E_s(\lambda) - E_{sky}(\lambda)$	4 (II), 2, 5 (III)	1,6,13
Water-Leaving Radiance $L_w(\lambda,\theta,\phi,\theta_o,\phi_o)$	2-4 (III), 2-4 (VI)	1,6,13
Remote Sensing Reflectance $R_{RS}(\lambda,\theta,\phi,\theta_o,\phi_o)$	2-4 (III)	1,6,13
Attenuation Coefficient $K(z,\lambda)$ for $E_d(z,\lambda)$ and $L_u(z,\lambda)$	2 (III), 2,3 (VI)	1,5,6,8,9
Ocean Bidirectional Reflectance Distribution Function BRDF	4 (III)	1,6,13
Aerosol Optical Depth $\tau_a(\lambda)$	5 (III)	1-3,4,6,7
Aerosol Phase Function $P_a(\lambda,\Psi)$	5 (III)	1-3,4,6,7
Absorbing Aerosol Height Profiles (LIDAR Profilometer)	TBD	1-3,6,7
Inherent Optical Properties		
Beam Attenuation Coefficient $c(z,\lambda)$	2 (IV)	1,5,6,8-10
Absorption Coefficient $a(z,\lambda)$	3, 4 (IV)	1,5,6,8-10
Backscattering Coefficient $b_b(z,\lambda)$	5 (IV)	1,5,6,8-10
Scattering Coefficient $b(z,\lambda) = c(z,\lambda) - a(z,\lambda)$	5 (IV)	1,5,6,8-10
Volume Scattering Function $\beta(z, \lambda,\Psi)$	5 (IV)	1,5,6,8-10
Particle Absorption Coefficient $a_p(z,\lambda)$	4 (IV)	1,5,6,8,9
Dissolved Material (CDOM) Absorption Coefficient $a_g(z,\lambda)$	4 (IV)	1,5,6,8,9
Non-Pigmented Particle Absorption Coefficient $a_d(z,\lambda)$	4 (IV)	1,5,6,8,9
Phytoplankton Absorption Coefficient $a_\phi(z,\lambda)$	4 (IV)	1,5,6,8,9

Table 3.2 Continued.

	Protocol Chapters (Volume)	Applications Keys
Biogeochemical and Bio-Optical Quantities		
Phytoplankton Pigment Composition (HPLC method)	2 (V)	1,5,6,8,9
Chlorophyll a and Phaeopigments Conc. (Fluorometric method)	3 (V)	1,5,6,8
Phycobiliprotein Concentrations	TBD	6,8
Coccolith Concentrations	1 (V)	1,5,6,8,9,12
Total Suspended Particulate Material (SPM)	1 (V)	5,6,8,12
Particle Size Distribution	TBD	5,8
Particulate Organic Carbon (POC)	1 (V)	5,8
Particulate Organic Nitrogen	1 (V)	5,8
Fluorescence Intensity, *in situ* profile $F(z)$	3 (V)	12
Ancillary Data and Metadata		
Latitude and Longitude	4 (I)	11
Date and Time (UTC)	4 (I)	11
Wave Height	4 (I)	12
Whitecap Conditions (fractional amount of surface)	4 (I)	12
Wind Speed and Direction	4 (I)	1-3,6,10,12
Surface Barometric Pressure	4 (I)	1,2,5
Cloud Cover (amount, and sun obscuration information)	4 (I)	6,10,12
Cloud Type	4 (I)	12
Secchi Depth	4 (I)	12
Water Depth	4 (I)	12
Conductivity and Temperature over Depth (CTD) $T(z)$, $S(z)$	4 (I)	9,10,12

Chapter 4

Field Measurements, Sampling Strategies, Ancillary Data, Metadata, and Data Archival: General Protocols

James L. Mueller

Center for Hydro-Optics and Remote Sensing, San Diego State University, California

4.1 INTRODUCTION

The purposes of this chapter are to present general background and protocols common to all combinations of validation measurements, analyses and data handling, and to collect protocols for field measurements not included in a separate volume of the document.

4.2 FIELD MEASUREMENTS

Chapter 3 of the present volume lists and describes the variables to be measured at each validation station. The "Required" variables (Table 3.1) represent the minimum set of field measurements made at a station, with others depending on the scientific application (Table 3.2) addressed on the particular research cruise.

A separate volume of this document is devoted to the protocols for the first three major categories of field measurements listed in Table 3.1: "Radiometric Quantities" are covered in Volume III, "Inherent Optical Properties" in Volume IV, and "Biogeochemical and Bio-Optical Quantities" in Volume V.

Protocols for "Ancillary Measurements and Metadata" are presented in Section 4.4 below.

4.3 VALIDATION SAMPLING STRATEGIES

The following discussion of bio-optical sampling protocols is organized into three subtopics: sampling for the initial and ongoing validation of a satellite radiometric system's performance, algorithm development and validation in Case-1 waters, and algorithm development and validation in Case-2 waters. The distinction between the first subtopic and the second two is clear-cut, but what precisely is meant by *Case-1*and *Case-2* water masses?

In its literature and reports, the ocean color research community has formally adopted definitions originally due to Morel and Prieur (1977), who stated:

"Case-1 is that of a concentration of phytoplankton [which is] high compared to that of other particles. The pigments (chlorophyll, [and] carotenoids) play a major role in actual absorption. In contrast, the inorganic particles are dominant in Case-2, and pigment absorption is of comparatively minor importance. In both cases, [the] dissolved yellow substance is present in variable amounts and also contributes to total absorption."

In practice, however, only those water masses where the CZCS-type blue-green ratio algorithms for phytoplankton pigment concentration (chlorophyll *a* plus pheopigment *a*) work reasonably well have been treated as *Case-1*. All other water masses have often been loosely lumped into the *Case-2* definition, albeit with considerable confusion over how to categorize coccolithophorid blooms, and waters in which strong concentrations of Gelbstoff vary independently from pigment concentration. By a strict interpretation of the original definition, both of these latter cases would be classified as Case-1.

In the present discussion of sampling protocols, Case-1 will be considered to refer to what might be called *ordinary open ocean Case-1* waters, wherein scattering and absorption are dominated by phytoplankton, pigments, and Gelbstoff concentrations, and where *global* blue-green color ratio algorithms for chlorophyll a concentration and $K(490)$ work well. Most areas in the deep ocean belong to this case. Water masses that do not satisfy these criteria will be grouped under the heading Case-2. Within Case-2, by this definition, water masses with a wide diversity of bio-optical characteristics will be found. Prominent subcategories include:

1. Coccolithophorid blooms, wherein the detached coccoliths dominate light scattering and remote sensing reflectance independently from pigment concentration;
2. Coastal areas, wherein DOM of terrestrial origin contributes a strong absorption component which does not co-vary with pigment concentration;
3. Phytoplankton blooms with unusual accessory pigment concentrations, *e.g.*, *red tides*, which require the use of special regional or local ocean color algorithms; and
4. Classical extreme Morel and Prieur (1977) Case-2 waters where optical properties are dominated by inorganic particles, with many possible variations in chemical and geometric characteristics.

It is important to recognize that some aspects of the water mass distinctions given above are dependent on the spectral regions in which measurements are to be made. Strong absorption at UV, red, and near-IR wavelengths requires the use of radiometric techniques similar to those required for Case-2 waters.

In addition to determining the bio-optical category and characteristics of a particular water mass, the validation sampling strategy must be concerned with spatial and temporal variability. Spatial and temporal variability in bio-optical properties will profoundly affect the validity of comparisons between satellite and in-water optical measurements. A single SeaWiFS instantaneous FOV measurement, for example, will integrate $L_W(\lambda)$ over approximately a square kilometer, or a larger area at viewing angles away from nadir. Furthermore, the location uncertainty for a single pixel may be several kilometers, except in near-shore areas where image navigation can be improved by using land-navigated anchor points.

Bio-optical profiles measured at a single station are representative of a spatial scale that is only a small fraction of a kilometer. Data from a grid of several station locations may be required to estimate the spatial averages of optical properties represented by a satellite pixel, or a block of pixels. Because the ship measurements over the grid are not instantaneous, temporal variability in bio-optical properties can add additional uncertainty to the comparisons. Aircraft radiometric observations can, conceptually, be used both to locate comparison sites away from areas of strong spatial variability and to document changes in the pattern of spatial variability over the period required for a ship to occupy all stations in a comparison grid.

Vertical stratification of water temperature, salinity, and density often affect the vertical structure of variability in bio-optical properties. This variability, in turn, affects the remote sensing reflectance. Vertical stratification of the water column becomes especially important in many Case-2 waters, where the top attenuation depth may be as shallow as 1 m to 2 m and the entire euphotic zone may be confined to less than 10 m depth. It is important, therefore, to minimize ship-induced disruption of vertical stratification in the water column. Whenever possible, the ship should be maneuvered as little as possible with its propellers and bow thruster, and the practice of backing down hard to stop quickly when on station should be strongly discouraged. If wind and sea conditions permit, the preferred method of approaching a station is to take enough speed off the ship to coast to a stop over approximately the last 0.5 Km of approach to the station. The approach should be planned to allow the ship to be turned, preferably using only the rudder, to place the sun abaft the beam, or off the stern, depending on where the radiometers will be deployed. It must be realized, however, that depending on wind and sea conditions, and a particular ship's hull and superstructure configuration, it may not be possible to maintain an acceptable orientation, with respect to the sun, while the ship is adrift. In these situations, some use of the engines to maintain an acceptable ship's heading may be unavoidable.

The chief scientist should also consult with the ship's captain and chief engineer to avoid, or at least minimize, overboard discharges while the ship is on station. Material from a ship's bilge or sewage treatment system can significantly change near-surface chemical and optical properties if discharged near the immediate site of a bio-optical profile, or water sample.

In some coastal areas, where a relatively transparent water mass overlies a highly reflective bottom, $L_W(\lambda)$ includes light reflected from the sea floor. These cases require special treatment of bottom reflectance effects, whether the local water mass regime is Case-1, Case-2, or a combination of both. Methods of measurement, experiment design, and sampling strategies to study bottom reflectance effects are beyond the scope of this revision to the ocean optics protocols. There is a significant current research effort focused in this area (Carder *et al*. 1993, Hamilton *et al*. 1993, and Lee *et al*. 1998, 1999), and new protocols in this topic area may be included in a future revision of this document.

The bottom reflection of areas with a water depth exceeding 30 m normally does not contribute to the water leaving radiance, $L_W(\lambda)$. Areas with a depth shallower than 30 m are flagged in the SeaWiFS level two data product. Pixels covering very turbid waters may, however, even be usable even in shallower areas. As a general rule, the water depth should be deeper than 2.5 attenuation lengths, 1/K(490), at all ocean color algorithm development and validation stations. The prime exception to this rule is in developing local ocean color algorithms where bottom reflectance contributions must be taken into account (Lee *et al*. 1998, 1999).

Initialization and Validation

Data intended for direct comparisons between ***exact normalized water-leaving radiances*** (Volume III, Chapter 4) $L_{WN}^{ex}(\lambda)$ determined from *in situ* measurements and from satellite data should usually be acquired in areas where bio-optical variability is known to be very small. This will ordinarily dictate that such data be acquired from optically clear and persistently oligotrophic Case-1 water masses. Potentially suitable sites include the northeastern Pacific central gyre off Baja, California (to the southwest), and the central Sargasso Sea. When planning validation cruise locations and timing, seasonal and regional cloud cover statistics should also be considered in order to maximize the likelihood of simultaneous satellite and shipboard observations. A Moored Optical BuoY (MOBY) is maintained and operated in a semi-oligotrophic site in the Northeast Pacific, near Hawaii, to provide continuous time-series radiometric comparisons with SeaWiFS, MODIS and other satellite $L_{WN}^{ex}(\lambda)$ estimates (Volume VI, Chapter 2; Clark *et al*. 1997).

A series of radiometric comparison stations should be made over a wide range of latitude in both the Northern and Southern Hemispheres, to look for evidence of cyclic thermal sensitivity affecting a satellite ocean color sensor. The spacecraft and instrument will be heated by sunlight throughout the descending (daylight) data acquisition segment of each orbit and will be cooled by thermal radiation while in the Earth's shadow throughout the remainder of the orbit. This cycling is likely to induce transient thermal gradients in the instrument, as well as a time varying cycle in the temperatures of its detectors and other components; these thermal variations could affect the spectral bandpass or responsivity of one or more of its channels. Unfortunately, a set of stations covering the full range of latitudes cannot all be sited in regions where mesoscale variability in ocean optical properties can be neglected.

As when acquiring data for developing and validating Case-1 bio-optical algorithms (see below), a significant effort must be exerted to quantify spatial variability in normalized water-leaving radiance. When possible, airborne radiometer data, in combination with careful characterization of atmospheric aerosol and cloud conditions, should be employed to augment shipboard radiometry at the stations selected for this aspect of the validation. If aircraft support is not available, semi-synoptic shipboard transects covering a $20 \times 20\ Km^2$ grid should be used to characterize spatial bio-optical variability near a sampling station (Clark *et al*. 1997).

The minimum set of variables to be measured for "match-up" validation analyses are those identified as "Required" in Table 3.1(Volume I, Chapter 3). Measurements used to calculate normalized water-leaving radiance for direct comparison to satellite sensor radiances must be made under cloud-free conditions and within five minutes of the satellite overpass.

Case-1 Water: Sampling Strategies

In open-ocean oligotrophic water, it is usually practical to assume that a station is in a Case-1 water mass, although some caution must be taken to detect coccolithophorid blooms and suspended coccoliths. In more turbid coastal transition regimes, however, the classification of the local water mass as Case-1 or Case-2 may be less obvious. In this environment, moreover, Case-1 and Case-2 water masses may both be present in the domain sampled by a ship. One example of this situation would be Case-1 water within an eddy-like intrusion from offshore into coastal areas normally occupied by Case-2 water masses. Another would be Case-2 waters in a major river plume intruding into an ambient Case-1 water mass regime. In general, a water mass may be categorized as Case-1 if:

1. Gelbstoff [Colored Dissolved Organic Matter (CDOM)] absorption at 380 nm, a_g (380), is less than $0.1\ m^{-1}$;
2. Total Suspended Particulate Matter (TSM) concentration is less than 0.5 mg L^{-1} (dry weight);

3. measured $L_{WN}(\lambda)$ values, used in the ocean color Case-1 algorithm, predict measured fluorometric chlorophyll *a* concentration within 35 %; and

4. measured $L_{WN}(\lambda)$, used in the ocean color algorithm, predicts measured remote sensing $K(490)$ within 20 %.

The determination of criterion 2 above (Doerffer pers. comm.) will ordinarily require retrospective analysis. On the other hand, *in situ* $a_g(z, 380)$ profiles (*e.g.* using an AC9 – see Volume IV, Chapter 3), radiometric profiles, and fluorometric pigment samples can ordinarily be analyzed on board to allow determination of criteria 1, 3 and 4 shortly after the samples are acquired.

Ocean color Case-1 algorithm development and validation requires measurements from Case-1 water masses spanning a wide range of optical properties and phytoplankton pigment concentrations. In optically transparent low-chlorophyll oligotrophic water masses, spatial variability is usually small and a station location and sampling strategy like that discussed above under *Initialization and Validation* is appropriate.

In high-chlorophyll mesotrophic Case-1 water masses with increased turbidity, mesoscale and smaller scale variability is often significant. In very productive Case-1 water masses, station placement and many other aspects of sampling schemes are similar to those discussed below under *Case-2 Waters: Sampling Strategy*. At algorithm development stations, where measurements need neither be coincident with, nor matched to, satellite observations, it will be necessary to characterize spatial and temporal variability only over the relatively short scales distinguishing the separate in-water radiometric, optical, and pigment measurements. Airborne ocean color, or LIDAR, characterizations of spatial variability in the vicinity of these stations will not usually be essential, although such additional information may be very helpful.

At stations where data are acquired for algorithm validation, and where a match to concurrent satellite ocean color measurements is required, it will be necessary to determine the patterns of spatial variability over a domain extending approximately 20 x 20 Km^2 centered at the station, and to place the ship in a 2 x 2 Km^2 domain over which $K(490)$ and chlorophyll concentrations vary less than 35 % about the mean. Within a few hours before and after a satellite overpass, in-water measurements should be made at several random locations to characterize variability within the 2 x 2 Km^2 validation comparison site. In some cases, it may be possible to determine spatial variability adequately from ship station data and alongtrack measurements alone. One approach is to measure the alongtrack profile of *in situ* chlorophyll *a* fluorescence at a depth of approximately 3 m, calibrated by filtered samples to determine chlorophyll *a* concentration at 15 min intervals (Volume V, Chapters 1 and 3). The model of Gordon *et al*. (1988) may then be used to estimate $L_{WN}(\lambda)$ from the alongtrack chlorophyll profile (Clark *et al*. 1997). In regions of strong mesoscale variability, concurrent aircraft ocean color, or LIDAR, measurements are also valuable as a guide for selecting the ship's location, and as a basis for spatially extrapolating the in-water measurements to match the much coarser resolution of the satellite ocean color measurements.

Case 2 Waters: Sampling Strategies

Although coastal and continental shelf areas comprise only 10 % of the total ocean area, they provide roughly half of the oceanic new production and most of the sequesterable DOC (Walsh *et al*. 1981). These areas are typically higher in phytoplankton pigment concentration, and may include colored terrigenous constituents such as CDOM and suspended sediments. In these *Case-2* waters, the global color ratio algorithms break down because two or more substances with different optical properties are present which do not co-vary with chlorophyll a concentration. These might be waters with exceptional plankton blooms (such as red tides), areas discolored by dust transported by the wind from deserts into the sea, or coastal areas influenced by river discharge of mineral and organic suspended materials, and Colored Dissolved Organic Materials (CDOM, *i.e. gelbstoffe*) such as humic acids.

It is not always easy to decide to which case a water mass belongs. As a starting point, the water belongs to Case-2 if any of the four Case-1 criteria set forth above, are not satisfied. For Case-2 waters defined by any one of these criteria, it remains a further problem to determine the specific bio-optical characteristics that distinguish it from Case-1. Case-2 sampling must usually include both the “Required” and “Highly Desired” variables, as identified in Table 3.1 (Volume I, Chapter 3), plus SPM. For example, it may be necessary to determine complete pigment composition and other optically important characteristics of exceptional phytoplankton blooms for such planktonic groups as *Coccolithophorids*, *Trichodesmium*, diatoms, cyanobacteria, or dinoflagellates.

To achieve valid comparisons between the ship and satellite data, sharp horizontal gradients and sub-pixel patchiness must be avoided, and accurate image navigation requires land anchor points near the study site. Suitable landmarks are usually available in near-shore coastal waters. The other conditions are difficult to meet in Case-2 water masses, where mesoscale and sub-mesoscale variability is typically very strong. Sub-pixel variations of no more than ± 35 % of the mean pixel chlorophyll will be tolerated, but variability must be measured and taken into account statistically in the analysis (see below).

From the above generalities, it is clear that significant problems are encountered in near-shore coastal waters characterized by small-scale patchiness and dynamic variability due to tidal currents. A particular problem occurs in the shallow areas that are influenced by strong tidal currents - areas that are normally well mixed during part of the tidal cycle. In the slack water tidal phase, however, a vertical gradient of the suspended matter concentration may form, which may cause problems in relating water-leaving radiance to the concentration of suspended matter. During calm periods with strong insolation, even water that is normally well mixed can become stratified. In these cases, the formation of very dense phytoplankton blooms, such as red tides, can be observed. Such blooms will occur in coastal seas when nutrient concentrations are elevated by the influx of river water. In these circumstances, it is especially critical to avoid disturbing the vertical stratification of the water column with the ship's propellers.

One approach to sampling in this environment has been suggested by R. Doerffer (pers. comm.). In order to get a good statistical base, water samples are first taken in a random order within the area under research. The concentrations derived from the satellite image data are then compared with the ground truth data by statistical parameters, such as the mean, median, standard deviation, and the shapes of histograms (frequency distribution). For this type of statistical comparison, only sections of satellite images that match the area covered by the ship should be analyzed. Water samples and satellite data should also be temporally concurrent within the same tidal phase to avoid biases due to temporal variability. In these regimes, analyses to validate algorithms cannot be based on satellite ocean color data directly, but must instead be based on water-leaving radiance spectra measured *in situ* (Volume III, Chapter 2) or from above the water surface (Volume III, Chapter 3). This approach has the advantage that water samples and radiance spectra are taken nearly simultaneously.

Using either flow-through pumping systems, or systems towed outside the ship's wake, fluorometry can be used to assess chlorophyll patchiness if frequent, *i.e.* every 10 min to 15 min, chlorophyll fluorescence-yield calibration measurements are performed. Towed absorption, scattering, reflectance, and beam transmission meters can also be used to characterize spatial variability. Within a few hours of the overpass, the ship should occupy several stations at random locations within a 2 x 2 Km^2 area central to the area selected for comparison with satellite data. Sampling stations placed across a tidal front during a satellite overpass may help to identify two different water masses, even when the front has moved. Comparisons between *in situ* and satellite data in patchy coastal areas may be enhanced by using horizontal radiance profiles measured from an aircraft flying at low altitude (Volume VI, Chapter 4). Subsets of such airborne profiles allow direct comparisons with shipboard data. A corresponding profile may then be extracted from the satellite image data for a direct comparison to the aircraft trackline profiles. In Case-2 situations, such direct radiometric comparisons are valuable for validating and tuning local algorithms, but are not appropriate for satellite ocean color sensor system validation *per se*.

To validate ocean color atmospheric corrections, water-leaving radiances measured *in situ* from the ship should be compared with those derived from the satellite data. Sample matching problems aside, Case-2 waters are often characterized by strongly varying patchiness in optical properties, pigment concentrations, and remote sensing reflectance at spatial scales smaller than a single pixel resolution of any of the current generation of ocean color sensors. Because of the nonlinear relationship between absorption by pigments, through $b_b(\lambda)/a(\lambda)$, and *exact normalized remote-sensing reflectance* $L_{WN}^{ex}(\lambda)/\overline{F}_o(\lambda)$ (Volume I, Chapter 2 and Volume III Chapters 3 and 4), the pigment concentration derived from spatially averaged satellite radiance data will systematically underestimate the true spatial average concentration by as much as a factor of 2 when sub-pixel variability is significant. It is, therefore, essential to describe sub-pixel scale variability in Case-2 waters both statistically and in terms of organized structure. Such a description may be accomplished through rapid sampling at closely spaced ship stations in combination with airborne ocean color or LIDAR measurements - trackline data from low altitudes and high-resolution imagery from high altitudes are both acceptable for this purpose (Volume VI, Chapter 4).

Absorption coefficients are large enough in all Case-2 waters to require instrument self-shading corrections to $L_u(0^-, \lambda)$, even though the correction model (Gordon and Ding 1992) has been experimentally verified only for the case where $a(\lambda)r$ is less than 0.1 (Volume III, Chapter 2, Section 2.4). In extreme Case-2 waters, large values of

spectral absorption may confine the first optical attenuation depth to the top 1 m to 2 m, where it is difficult to measure remote sensing reflectance *in situ*. Such short absorption scale lengths lead to instrument self-shading effects in $L_u(0^-,\lambda)$ that are correctable within ~5 % only for instruments with diameters no larger than approximately 1 cm (Gordon and Ding 1992). Radiometers with such a small shadow cross section are conceptually feasible, and a few prototype instruments exist which may be suitable, but they are not commercially available, and self-shading sensitivities have not yet been experimentally verified for these extreme conditions. In these extreme cases, direct *in situ* measurements of $a(\lambda)$, $c(\lambda)$ and $b_b(\lambda)$ (Volume IV, Chapters 2 through 5), together with $L_{WN}(\lambda)$, or $R_{RS}(\lambda)$, determined from above-water radiometric measurements (Volume III, Chapter 3), may provide the only practical means of developing and validating semi-analytic Case-2 algorithms. This topic remains an important area for near-term research and development.

4.4 ANCILLARY MEASUREMENTS AND METADATA

The "Required" and "Highly Desired" ancillary measurements and metadata are listed in Table 3.1 (Volume I, Chapter 3). Ancillary observations are often of key importance in flagging and interpreting apparently aberrant data. In addtion, some of ancillary measurements are essential for corrections to optical measurements, for example the Temperature and Salinity dependence of spectral absorption by pure water must be used in the processing and analysis of AC9 data (Pegau and Zaneveld 1993; Pegau *et al*. 1997). Metadata peculiar to a particular type of measurement, such as instrument calibration information, serial numbers, etc., are specificied in the protocols for making those measurements. The present section identifies recommended methods for acquiring and recording the information and data of more general applicability.

Logbooks

The person, or group, making a particular set of measurements normally maintains a separate logbook to record complete metadata unique to a particular instrument, including names of measurement and dark reference data files. It is the chief scientist's responsibility to also maintain a master logbook in which essential metadata (event, time, location) and general environmental conditions are recorded to link all measurements and samples acquired at each station. At the end of each cruise, the chief scientist should also obtain a photocopy of the ship's bridge log from the vessel's master.

Wind Speed and Direction

If possible, anemometer measurements of wind speed and direction should be recorded continuously throughout each station, and underway between stations if alongtrack data are recorded. As a precaution, the wind speed and direction should be read and recorded manually in the master and individual instrument log entries for each measurement made during a station. If the only available anemometer is not digitally recorded, these manual log entries will obviously be the only record available.

Barometric Pressure

Surface barometric pressure should be read from both the ship's barometer, and from any barometer that is part of an automatically recorded meteorological system, and recorded in the chief scientist's master logbook. This information should be manually logged at the beginning, end, and hourly during sampling at each station. If possible, it is also desirable to digitally record barometric pressure, along with wind speed and direction, throughout each station and while steaming between stations, if other alongtrack meteorological data are recorded.

Cloud Conditions

The percent of the sky covered by clouds should be logged at the time of each measurement event. Identification of cloud types, including such comments as "thin cirrus", is "Highly Desired", but not "Required" (Table 3.1 in Volume I, Chapter 3). It is also very useful, for broken and partial overcast conditions, to comment on the relationship between locations of clouds and the zenith and azimuth angles of the sun and satellite, and whether the sun is occluded. For validation cruises, predictions of approximate satellite and solar zenith and azimuth angles for given locations and days are available on request from the SIMBIOS Project Office.

All-sky photographs, using a digital camera equipped with a fisheye lens are useful documentation of sky conditions. Digital photographs of segments of the sky, using a camera with a smaller field-of-view lens, are also useful if annotated with zenith and azimuth pointing angles.

Wave Height

The overall wave height, peak to trough in m, estimated visually by a trained and experienced observer is adequate for purposes of these protocols. As is explained in any introductory textbook on general oceanography, this type of height estimate closely corresponds to *Significant Wave Height*, defined as the average of the highest one-third waves in a 20 min record of measured wave amplitudes. More sophisticated measurements of ocean surface wave characteristics are beyond the scope of these protocols. Where the protocols for a particular measurement require it, *e.g.* above-water remote-sensing reflectance protocols (Volume III, Chapter 3) or computation of $L_{\mathrm{WN}}^{\mathrm{ex}}(\lambda)$, the wave slope spectrum is calculated from wind speed. Estimates of the percent of the surface covered by whitecaps are also useful as comments, but this may usually be adequately estimated from wind speed as well. Digital photographs of the sea surface conditions are useful documentation of sea state and whitecap conditions at the time of radiometric measurements.

Secchi Depth

A *Secchi Disk* is a white circular disk, approximately 25 cm in diameter, attached to a line marked with a stripe at 25 cm intervals and a broader stripe (or double stripe) at each full meter. A lead weight (~5 Kg) is attached to the bottom of the rig to maintain the disk in a horizontal orientation as it is lowered and raised through the water. The disk should be lowered through the ship's shadow on the side away from the sun to reduce surface glint. The observer pays out the line, lowering the disk until it just disappears from his view and then raises it until just the depth where it again becomes discernable. The depth indicated by the line markings at the water surface when the disk disappears from the observer's view is recorded as Secchi depth in m.

At depths shallower than Secchi depth, the high reflectance of the white disk (~90 %) produces a target with strong visual contrast to the lower reflectance (~2 %) of the ambient water column. As the disk is lowered deeper in the water, irradiance illuminating the disk is reduced and the light reflected from it is also attenuated during its transmittance to the sea surface. Therefore, the apparent contrast between the target and surrounding water is reduced with increasing depth, until at Secchi depth, the contrast disappears between the target and water column. The reader interested in a more quantitative analysis and interpretation of Secchi depth should begin with the treatment by Preisendorfer (1986).

Secchi depth should be taken at least once at each station and recorded in the chief scientist's master log, and in the separate logbooks maintained for radiometric, IOP and CTD-Rosette profiles. It is the author's experience that in optically deep water masses, Secchi depths, in m, display a strong linear correlation with $K(490)^{-1}$, also in m. $K(490)$ is the diffuse attenuation coefficient $K_d(z,490)$ averaged over the top diffuse attenuation length, and its inverse corresponds to the depth at which measured $E_d(z,490)$ is 37 % of $E_d(0^-, 490)$. A useful quality control procedure is to plot Secchi depth against $K(490)$ for every station on a cruise. Departures from a strong linear trend between these variables are indicative of either suspect data, or of anomalous conditions. For instance, if bottom reflectance is significant at a station, then the Secchi depth from that station will be significantly less than that predicted by its deep water correlation with $K(490)^{-1}$. This occurs because the ambient background brightness is enhanced by light reflected by the bottom, and the disk's contrast disappears at a shallower depth that would have occurred in deeper water with the same $K(490)$.

Conductivity, Temperature and Depth (CTD) Profiles

Although Temperature $T(z)$ and Salinity $S(z)$ profiles measured with a CTD are listed as only "Highly Desired" in Table 3.1 (Volume I, Chapter 3), these measurements are essential for corrections to *in situ* absorption measurements (Volume IV, Chapter 3). Moreover, the availability of a combined CTD and Rosette-sampling system strongly affects the quality of discrete water samples acquired to measure phytoplankton pigment concentrations, which are important "Required" measurements. This is particularly true if the CTD+Rosette system is also equipped with a single-wavelength beam transmissometer to measure, *e.g.*, $c(z, 660)$ (Volume IV, Chapter 2), and a fluorometer to measure *in situ* chlorophyll *a* fluorescence intensity $F(z)$ (Volume V, Chapter 3). The recommended sampling protocol is to measure, and display in real time on a computer monitor during the downcast,

profiles of $T(z)$, $S(z)$, the sea water density anomaly $\sigma_t(z)$, $c(z,660)$, and $F(z)$. The profile of $\sigma_t(z)$ provides the best indicator of the depth of the mixed layer and strength of the underlying pycnocline. Structure in the $T(z)$ and $S(z)$ profiles may be used to indicate the presence of interleaving water masses with possibly different bio-optical origins and characteristics. The $F(z)$ profiles will identify depths of subsurface maxima and strong gradient features in the chlorophyll profile. The $c_p(z,660) = c(z,660) - c_w(z,660)$ profile will reveal depths of gradients, maxima, and minima in the concentration of suspended particulates. This graphical information can be used to quickly select appropriate depths at which water samples will best represent the bio-optical structure of the water column. Finally, during the upcast, the CTD+Rosette package is stopped at each selected depth, a selected bottle is closed, and its identification number and digitally displayed depth from the CTD unit are recorded in the water sample log.

The combined CTD, transmissometer and fluorescence profiles should be measured in conjunction with, preferably immediately before and after, the irradiance and radiance profile measurements. This is feasible, because more than one cast is typically required to obtain enough water samples for all measurements on each station. The $c_p(z,660)$ and $F(z)$ profiles are very useful as guides for, and constraints on, the determinations of attenuation coefficients $K(z,\lambda)$ from the radiometric profiles (Volume III, Chapter 2). These data are also useful information for analyses to develop and validate pigment and primary productivity algorithms. Vertical profiles of CTD should be measured to at least the depth of the deepest bio-optical profile. If the station schedule will permit it, sections of CTD casts extending to 500 m, or deeper, will be useful for computing relative quasi-geostrophic currents and shear that may affect the advection and mixing of bio-optical properties during a cruise.

If possible, a few deep (1,500 m depth or greater) CTD and bottle sample profiles should be made during each cruise to obtain data for calibrating the CTD's conductivity probe. During these *CTD calibration casts*, water samples should be taken at depths where the vertical gradient of salinity is very small. This practice will minimize errors in the conductivity calibration resulting from the spatial separation of the water bottle and CTD profile. The bottled salinity samples may be stored for post-cruise analyses ashore at a laboratory equipped with an accurate salinometer and IAPSO Standard Seawater, if suitable equipment and standard water are not available aboard the ship (Volume II, Chapter 1, Section 1.9).

Each CTD profile should be prefiltered to remove any depth reversal segments resulting from violent ship or hydrowire motions. This will remove many instances of salinity spiking, an artifact which occurs when water temperature changes at a faster rate than the conductivity probe can follow. The CTD data should then be processed to profiles of potential temperature (^oC), salinity (Practical Salinity Units [PSU] based on the Practical Salinity Scale of 1978, PSS78), and density (kg m^{-3}) using the algorithms that have been endorsed by the United Nations Educational, Scientific, and Cultural Organization (UNESCO)/SCOR/International Council of Exploration of the Seas (ICES)/IAPSO Joint Panel on Oceanographic Tables and Standards, and also by SCOR Working Group 51 (Fofonoff and Millard 1983).

At this stage, each set of CTD profiles should be carefully examined to detect any significant static instability artifacts resulting from salinity spiking. After any such major artifacts are removed by editing, the data should be further smoothed by averaging temperature and conductivity data into 2 m depth bins, and the final profiles of salinity, density, and other derived parameters should be recomputed using the smoothed CTD profile.

For any hydrographic station, descriptive hydrographic analyses should include *T-S* profile characterizations of water masses. Features in the density profile that appear to be related to physical mixing and stability should be compared with features in the corresponding bio-optical profiles. CTD profiles from horizontal transects (*i.e.*, two-dimensional grids) should be used in the computation of two-dimensional sections, or three-dimensional gridded arrays, for such variables as geostrophic currents, temperature, salinity, and the density anomaly σ_t. These analysis products, together with corresponding two- or three-dimensional representations of bio-optical variability, can be used to estimate the relative importance of advection and isopycnal mixing in redistributing or modifying upper ocean optical properties during a cruise.

Metadata

For each water sample and measured variable (of all categories) listed in Table 3.1 (Volume I, Chapter 3), it is critical to record the date, time (UTC), and geographic position (latitude and longitude in decimal degrees to the nearest 0.001^o) of its acquisition or measurement. Position and time metadata should be obtained using a Global Positioning System receiver, if possible.

Depths of measurements made with profiling instruments are usually recorded electronically in the profile data records and files. If measurements are made at depths determined by means other than a pressure transducer integrated with the data acquisition system, then the source of that information must be logged (*e.g.* reference to another file containing time synchronized depth records from an independent instrument on the same package). In the case of a visually read depth scale (*e.g.* line markings, or a rigid scale attached above an instrument), as is sometimes done to obtain depths with uncertainty < 1 cm in very turbid Case-2 waters under calm conditions, each individual depth must be identified with the measurement and entered in a logbook.

The depth from which each water sample is acquired must be recorded in a log, together with all other information required for each measurement to be made from that sample, including pigments (Volume V, Chapters 2 and 3) and spectrophotometric absorption measurements (Chapter 15). This depth is ordinarily read from the CTD system attached to a rosette sampler. If a CTD, or other instrument equipped with a pressure transducer, and rosette sampler are not used (*e.g.* as with bottles hung directly on the hydro-wire), then the method used to determine bottle depth on closing must be fully described, together with an estimate of the uncertainty in each depth, in comments accompanying the data.

Wire angles should be logged at different depths during each instrument and bottle sampling cast. These entries are critically important for radiometric casts, and for bottle casts when a CTD+Rosette system is not used.

The depth of the water column should be read from the vessel's fathometer and recorded in the log. If the water depth exceeds the range of the fathometer, the recorded depth should be taken from a navigation chart. The distance off the ship of a profiling radiometer, and its direction, and that of the sun, relative to the ship's heading provides an important indication of the likelihood that ship shadow effects may be present in the data. Similarly, the ship's heading relative to the sun may help identify possible shading (or reflection) artifacts in $E_S(\lambda)$ if the shipboard reference radiometer cannot be mounted higher than all masts, antennas, and superstructure elements. It is usually adequate to simply enter a sketch in the log showing the sun and package positions relative to the ship. Of course if the ship's compass heading (in degrees – Magnetic or True) is recorded, the solar azimuth and zenith may be easily computed from the time and position metadata.

4.5 DATA ARCHIVAL

The SeaWiFS and SIMBIOS Project Offices jointly maintain the SeaWiFS Bio-Optical Archive and Storage System (SeaBASS) as a resource for collecting in one place, in a readily accessible format, the full scope of data covered by the this protocol document. Scientists whose ocean color research is supported under NASA's SIMBIOS and other ocean color research programs are required to submit their data to SeaBASS for archival, and data sets are regularly obtained from other members of the international ocean color research community as well. Access to data submitted SeaBASS is initially restricted, but are released to the public at large 3 years following acquisition, and often sooner.

At this writing, the SeaBASS data and access policies, data file formats, data submission and quality control procedures, architecture and relational data base management system design, and online data access resources are described by Werdell and Bailey (2002). This document, which is jointly promulgated by the SeaWiFS and SIMBIOS Project Offices supercedes and replaces the more limited SeaBASS information and requirements that were previously included in the Ocean Optics Protocols (Werdell *et al.* 2002a, 2002b). Future publications that revise and update the SeaBASS information presented in Werdell and Bailey (2002) will also be issued independently from the ocean optics protocols.

REFERENCES

Carder, K.L., P. Reinersman, R. Chen, F. Muller-Karger, and C.O. Davis, 1993: AVIRIS calibration and application in coastal oceanic environments. *Remote Sens. Environ.,* **44**: 205--216.

Clark, D.K., H.R. Gordon, K.J. Voss, Y. Ge, W. Broenkow, an C.C. Trees, 1997: Validation of atmospheric correction over oceans. J. Geophys. Res., 102: 17,209-17217.

Fofonoff, N.P., and R.C. Millard, Jr., 1983: Algorithms for computation of fundamental properties of seawater. *UNESCO Tech. Papers in Marine Science*, **44**, UNESCO, 53 pp.

Gordon, H.R., and K. Ding, 1992: Self shading of in-water optical instruments.*Limnol. Oceanogr.,* **37**: 491--500.

Gordon, H.R., O.B. Brown, R.H. Evans, J.W. Brown, R.C. Smith, K.S. Baker, and D.K. Clark, 1988: A semi-analytic radiance model of ocean color. *J. Geophy. Res.* **93**(D9): 10,909-10,924.

Hamilton, M.K., C.O. Davis, W.J. Rhea, S.H. Pilorz, and K.L. Carder, 1993: Estimating chlorophyll content and bathymetry of Lake Tahoe using AVIRIS data. *Remote Sens. Environ.*, **44**: 217--230.

Lee, Z.P., K.L. Carder, C.D. Mobley, R.G. Steward and J.S. Patch, 1998: Hyperspectral remote sensing for shallow waters: 1. A semianalytical model. *Appl. Opt*., **37**(27): 6329-6338.

Lee, Z.P., K.L. Carder, C.D. Mobley, R.G. Steward and J.S. Patch, 1999: Hyperspectral remote sensing for shallow waters: 2. Deriving bottom depths and water properties by optimization. *Appl. Opt.*, **38**(18): 3831-3843.

Morel, A., and L. Prieur, 1977: Analysis of variations in ocean color. *Limnol. Oceanogr.,* **22**: 709--722.

Pegau, W.S. and J.R.V. Zaneveld, 1993: Temperature dependent absorption of water in the red and near infrared portions of the spectrum. *Limnol. Oceanogr*., **38**(1): 188-192.

Pegau, W.S., D. Gray and J.R.V. Zaneveld, 1997: Absorption and attenuation of visible and near-infrared light in water: dependence on temperature and salinity. Appl. Opt., **36**(24): 6035-6046.

Preisendorfer, R. W., 1986: Secchi disk, science: Visual optics of natural waters. *Limnol. Oceanogr.,* **31**(5): 909-926.

Werdell, P.J. and S.W. Bailey, 2002: The SeaWiFS Bio-Optical Archive and Storage System (SeaBASS): Current Architecture and Implementation. Fargion, G.S. and C.R. McClain [Eds.] NASA/TM-2002-211617. NASA Goddard Space Flight Center, Greenbelt, MD, 45pp.

Werdell, P.J. S.W. Bailey, and G.S. Fargion, 2002a: Seabass data protocols and policy. In: *Ocean Optics Protocols for Satellite Ocean Color Validation , Revision 3* (Chapter 18), Mueller, J.L. and G.S. Fargion [Eds.], NASA Tech. Memo. 2002/210004/Rev. 3, NASA Goddard Space Flight Center, Greenbelt, Maryland, 284-287.

Werdell, P.J. S.W. Bailey, and G.S. Fargion, 2002b: Appendix B: SeaBASS dta file format. In: *Ocean Optics Protocols for Satellite Ocean Color Validation , Revision 3*, Mueller, J.L. and G.S. Fargion [Eds.], NASA Tech. Memo. 2002/210004/Rev. 3, NASA Goddard Space Flight Center, Greenbelt, Maryland, 292-298.